# Cellulose Templated Synthesis of Calcined Zn-Al LDH/AgI Composite Catalyst for Effective Removal of Cr(VI) from wastewater

A thesis submitted to

The Department of Materials Science and Engineering

School of Mechanical, Chemical and Materials Engineering

Presented in Partial Fulfillment of the Requirement for the Degree of Master in Materials Science and Engineering

Office of Graduate Studies

Adama Science and Technology University

**Simachew Andualem Mekonnen**

**ID: PGR/18058/11**

Advisor: Dr. Osman Ahmed

Co. Advisor: Dr. Belay Brehane

Adama

July /2020

# Cellulose Templated Synthesis of Calcined Zn-Al LDH/AgI Composite Catalyst for Effective Removal of Cr(VI) from wastewater

Simachew Andualem Mekonnen

Advisor: Dr. Osman Ahmed

Co. Advisor: Dr. Belay Brehane

Thesis Submitted to

Department of Materials Science and Engineering-

School of Mechanical, Chemical and Materials Engineering

Presented in Partial Fulfillment of the Requirement for the Degree of Master in Materials Science and Engineering.

Office of Graduate Studies

Adama Science and Technology University

Adama

July/2020

**Approval of Board of Examiners**

We, the undersigned, member of the Board of Examiners of the final open defense by Mr. Simachew Andualem Mekonnen have read and evaluated his thesis entitled "Cellulose Templated Synthesis of Calcined Zn-Al LDH/AgI Composite Catalyst for Effective Removal of Cr(VI) from wastewater and examined the candidate. This is, therefore, to certify that the thesis has been accepted in partial fulfillment of the requirement of the Degree of Master of Science.

| | | |
|---|---|---|
| _____ | _____ | _____ |
| Supervisor /Advisor | Signature | Date |
| _____ | _____ | _____ |
| Chairperson | Signature | Date |
| _____ | _____ | _____ |
| Internal Examiner | Signature | Date |
| _____ | _____ | _____ |
| External Examiner | Signature | Date |

## Declaration

I hereby declare that this MSc Thesis is my original work and has not been presented for a degree in any other university, and all sources of material used for this thesis have been duly acknowledged.

Name: _____

Signature: _____

This MSc Thesis has been submitted for examination with my approval as thesis advisor.

Name: _____

Signature: _____

Date of submission…….

# Acknowledgments

Above all, I would like to thank the almighty God, lord of creations for his endless grace and blessing me and also for giving me health, strength, opportunity, patience to complete with prospective ability to attain my task in this project thesis work.

I would like to thank my advisor Dr. Osman Ahmed for his indispensable, prompt help and invaluable effort in guiding and supervising during the course of this thesis. I treasure his advice which has contributed a great deal to the success of this work. Had it been not for his advice, the accomplishment of the thesis work would have been impossible. I would like to express my deepest thanks to my Co-Advisor Dr. Belay Brehane for his continuous support and guidance.

I want to thank and express my heartfelt gratitude to Adama Science and Technology University School of Mechanical, Chemical and Materials Engineering, Department of Materials Science and Engineering, for its great contribution providing me facilitation of laboratory which is a back bone of my work for the analysis of result. I would also like thank Dr. Dinseffa Mensur head of department MSE and Mr. Demeke Tesfaye laboratory technician for your creation of a conducive environment in the laboratory.

I would like to thank Defense University, college of engineering who gives this chance to study MSC program in Adama Science and Technology University with providing financial support to carry out this study.

My family (mother Elimnesh Bekele, wife Alem Kassahun) and my friends has countless help for me by encouraging me day and night from beginning to end of the job, thank you every body.

Last but not least, I would like to thank and show my respect to all my classmates who shared their helpful thoughts and ideas to support my work.

I dedicate this thesis to my family specially my Mother Elimnesh Bekele who has taught me values and excellence which has enabled me to reach at this point of study in the life.

# List of contents

Table of Contents page number

# List of Figures

# List of Abbreviations

CB----------Conduction Band

DPC----------Dyphenylcarbazide

DRS----------Diffusiblity Reflectance Spectroscopy

EDS----------Energy Dispersive X-ray Spectroscopy

HMs----------Heavy Metals

LDH----------Layered Double Hydroxide

MCC----------Micro-Cellulose

MMO----------Mixed Metallic Oxide

SCB----------Sugar Cane Bagasse

UV-vis----------Ultra-Violet Visible Ray

VB----------Valance Band

WHO----------World Health Organization

WWTT----------Waste-Water Treatment Technology

XRD----------X-ray Diffraction

# Abstract

*Environmental pollution is one of the big risk factor for social health problem around the world. Particularly, water pollution due to heavy metals is the widest challenges for the globe. Therefore, it needs to search not only efficient methods but also eco-friendly materials. In this work, cellulose was extracted from sugar cane bagasse used as a template for the synthesis of Zn-Al LDH. The resulting Zn-Al LDH was calcined at various temperatures (500- 950 $^{\circ}C$) to remove cellulose and to obtain porous ZnAl MMO. The obtained MMO composite was thoroughly characterized by powder x-ray diffraction (XRD), scanning electron microscopy (SEM), UV-Vis diffuse reflectance spectroscopy(DRS). The catalytic performance was evaluated and the result shows Zn-Al LDH calcined at temperature of 900 $^{\circ}C$ has better performance. Then, the AgI deposited on the ZnAl MMO for further enhancement of the photocatalytic reduction of chromium, Cr(VI). The catalyst with deposition of 40% AgI on ZnAl MMO (ZnAl MMO/AgI) reduced 87% of 20 ppm Cr(VI) solution within 90 min irradiation. However, a similar catalyst composition without cellulose was prepared reduce only 66% of 20 ppm Cr(VI) solution with in 90 min irradiation. Hence, using cellulose as a template and deposition of the appropriate amount of AgI on ZnO/$ZnAl_2O_4$ photocatalyst could enhanced the catalytic reduction of Cr(VI) solution under visible light source.*

***Keywords,*** *layered double hydroxide, calcined, semiconductor, cellulose, mixed metal oxide, composite, photocatalyst*

# 1 Introduction

## 1.1 Background

Environmental pollution is one of the big risk factor for social health problem around the world. Particularly, environmental pollutions occur in water resource is the biggest challenges for the globe. Recently, the pollution of water by heavy metals (HMs) such as Cr, Pb, Cd and dyes are a concern due to their highly toxicity and accumulation in aquatic habitats. This pollution chemicals or HMs oxides comes from several natural and human activities [1]. The growth of population rate, global modernization, and large quantities of industrial wastewater effluents containing hazardous dyes and heavy metal ions are the potential sources of water pollutions [2]. Hazardous dyes and heavy metal ions from paper, textile, printing, plastic, and electro-plate, leather tanning industries are being discharged into the water bodies, which cause a serious problem to human health, living organisms, and the ecosystem [3]. Particularly, heavy metals are mostly described as elements that have atomic weights between 63.5 and 200.6 and specific gravity greater than 5 $g/m^3$. Heavy metals such as copper (Cu), zinc (Zn), manganese (Mn), iron (Fe), nickel (Ni), molybdenum (Mo), and cobalt (Co) are necessary in biochemical micronutrients processes for living beings [4]. Particularly, the heavy metals such as chromium (Cr), lead (Pb), cadmium (Cd), mercury (Hg), and arsenic (As) are toxic [5]. These HMs even at trace amounts (parts per billion, ppb) are dangerous for human life because they are non-digestible and can bio-accumulate in the systems of human body. Among the hazardous heavy metals, hexavalent chromium (VI) is extremely available in wastewater from electroplating and metal finishing process, tannery facilities and pigment production, and chromium mining operations [6-8].

Highly soluble and toxic chromium anions ($HCrO_4$-, $Cr_2O_7^{2-}$) creates from discharge of Cr(VI) to the surrounding which cause carcinogenic and mutagenic diseases, like dermatitis, lung cancer, liver irritation and chronic ulcers to the society. Therefore, Cr(VI) is higher toxic than other HMs ions. In order to reduce the negative influence of Cr(VI) on environment and society health, it is highly necessary to reduce Cr(VI) in its nontoxic level Cr(III) in wastewater [9, 10].

A high number of adsorbents, such as activated carbon [11], functional synthetic polymers [12], chemical syntheses polysaccharides [13, 14], porous aluminosilicate [15], heterojunction metal oxide [16], and waste biomass [17] have been provided for removing Cr(VI) from polluted

solutions. In addition, layered double hydroxide (LDHS) materials are possible selective adsorbent due to their good stability, large specific surface area, and high ability for ion exchange [18]

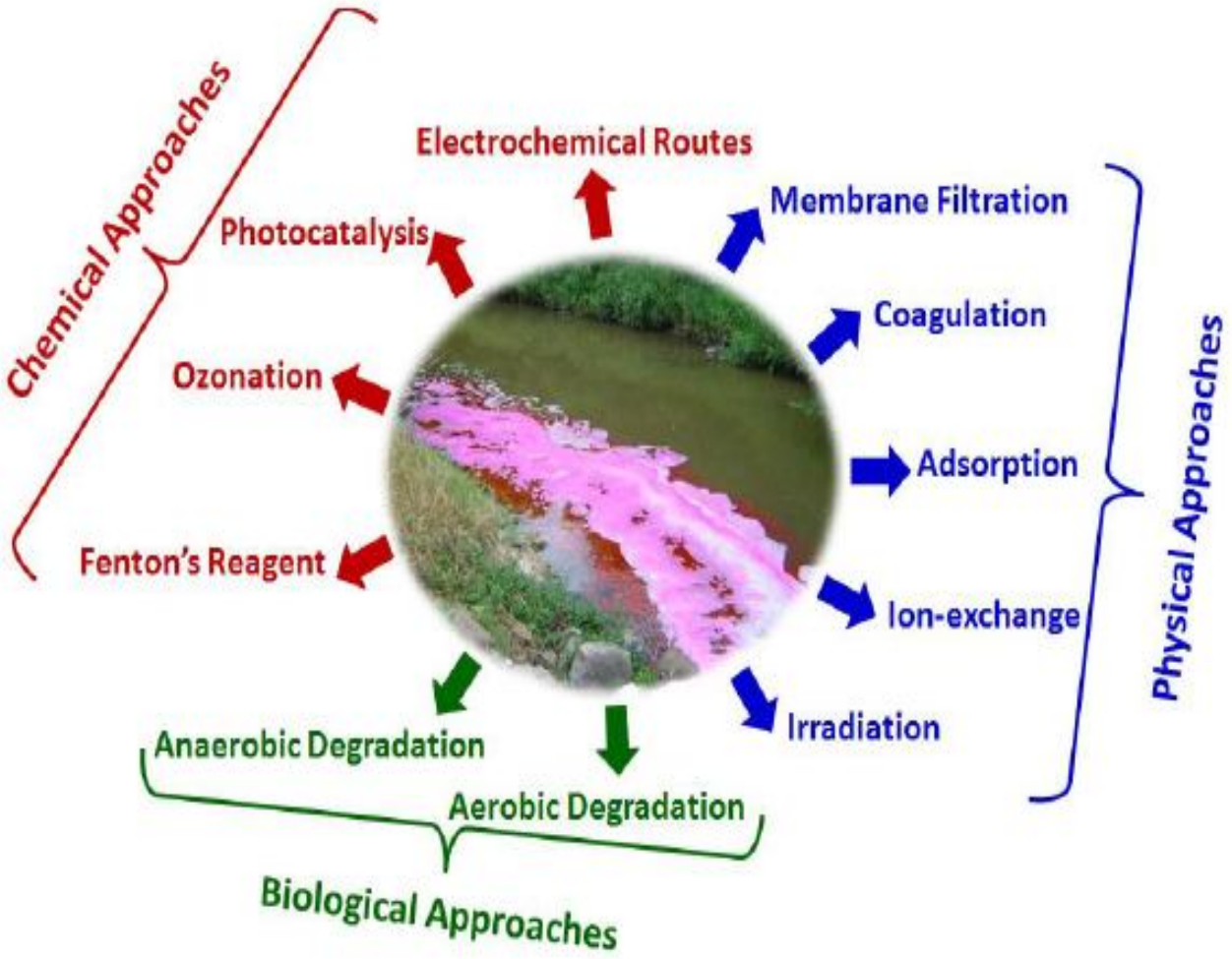


Figure 1. Chemical, biological, and physical approaches to remove or degrade pollutants in the wastewater [19].

LDHs are host and guest components obtaining metal hydroxide and water molecules of positively charged metal sheets with intercalated anion [20]. The arrangement of these compounds are derived from brucite structure materials, when the divalent cations changed by the trivalent cations. The general formula represented by $[M^{2+}_{1-x}M^{3+}_{x},(OH)_2]^{x+}[A^{n-}]_{x/n}.mH_2O$, where the divalent $M^{2+}$ and trivalent $M^{3+}$cations may be $Ni^{2+}$, $Mg^{2+}$, $Zn^{2+}$, $Fe^{3+}$,$Cu^{2+}$, $Al^{3+}$, $Co^{3+}$, $Ga^{3+}$ and the $A^{n-}$ is interlayer gallery anions (e.g. $CO_3^{2-}$, $SO_4^{2-}$, $NO_3^-$, $Cl^-$) can be like any inorganic or organic anion.

X is the molar ratio of $M^{3+}/(M^{2+}M^{3+})$, ranging from 0.2 to 0.33 in order to avoid the creation of undesirable phases, and m is the molar amount of co-interlayered water [21-23].

The removal efficiency of oxide ions was improved by the layered structure through induce of electron, inhibit recombination of $e^{-}$-$h^{+}$ and eliminating the aggregation of the particles [24]. LDH based materials have attracted choice of application for photocatalysis deposition as supporting materials. These show the feasibility of the material from the economic point of view. These materials are obtained by simple co-precipitation method using only inorganic precursors, for example calcinations [20, 25].

Many researches used adsorption/photocatalytic processes in the past to remove Cr(VI) from wastewater. Calcination at temperature between (400-550$^{0}$C) cause LDH to remove its moisture and hydroxyl, along with associated anions. Then it created poorly crystallized MMOs with high surface area. During rehydration process, its original layered structure partially recovered in the presence of oxyanions which is known as "a structure memory effect". As a result, calcinations can be further improving the adsorption efficiency of oxide ions such as Cr(VI). LDH materials with several transition element ions can behave as semiconducting materials [18, 23]. However, simultaneous application of photocatalysis and adsorption is still in the experiment stages. Photocatalyst reduction of Cr(VI) to Cr(III) using the semiconductor photocatalysis method has obtained desirable photocatalysis technology. Electron ($e^{-}$) and hole ($h^{+}$) are created throughout the photolysis proceed of the energy gap. These photo generated electrons and holes either recombined or applied in redox reactions. The photo- excited electrons transferred the reduction of Cr(VI).

The excited electrons to the conduction band during the organics materials degradation can attack oxygen ($O_2$) and create active form $H_2O_2$, $O_2\bullet$-, and •OH. The holes with extremely oxidizing ability can straightly take part in oxidizing water or oxidation degradation of organic to produce •OH· These generated active species $H_2O_2$, $O_2\bullet^{-}$, and •OH can fully degrade organic to $CO_2$ and water. Holes cannot be participated to reduce Cr(VI) to Cr(III) , and still create •OH from water oxidation, which may be oxidize Cr(III) to Cr(VI). Then, the photocatalytic reduction of Cr(VI)

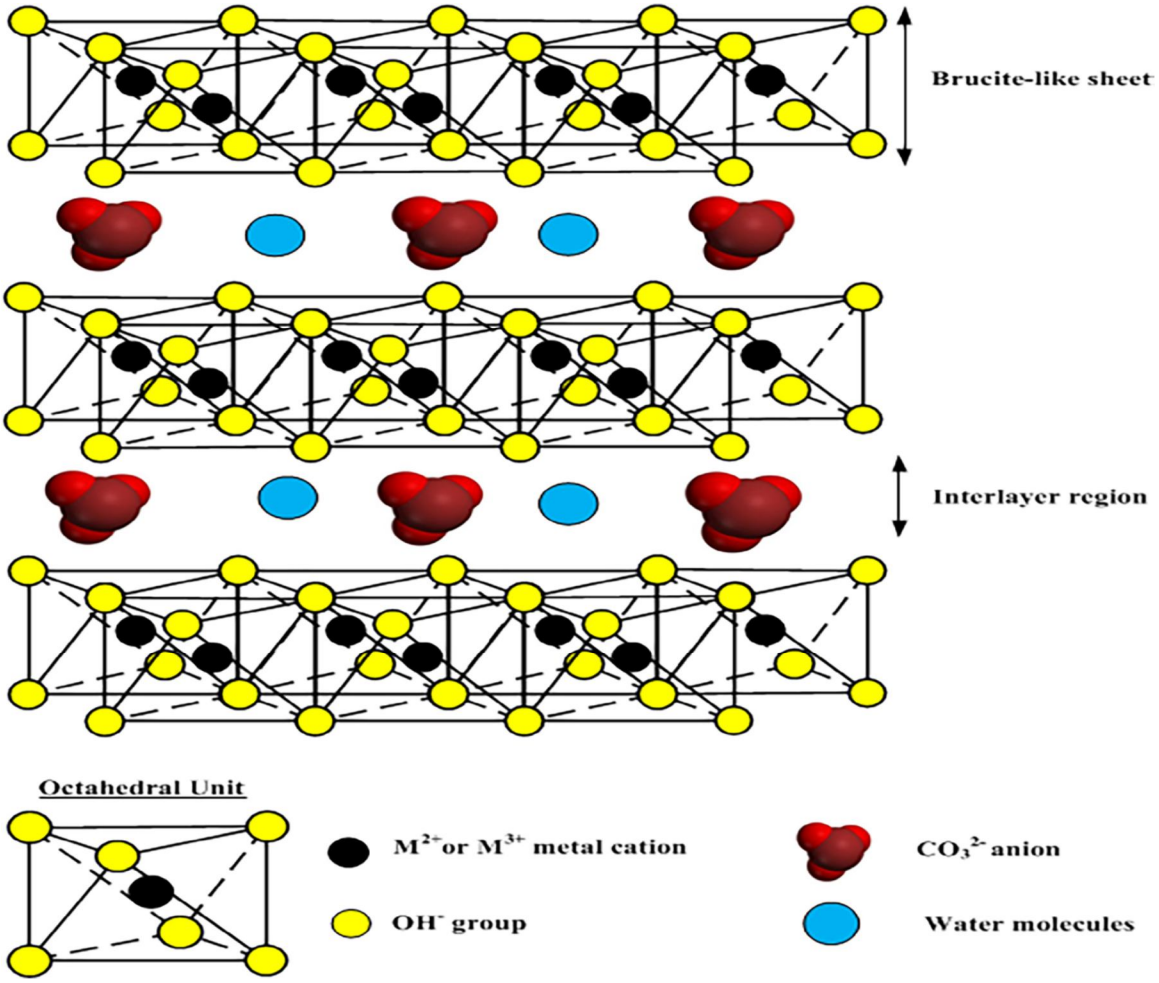


Figure 2. The structure of a layered double hydroxide with interlayer $CO_3^{2-}$ anions [26].

can be performed with the oxidation of organic couplings by imparting some organic pollutants in solution. However, organic pollutants generally exist concurrently in a real contaminated system of inorganic and heavy metal ions [27, 28]. In the previous works, Zn/Al LDH with $TiO_2$ has done with UV light source [29]. However, the efficiency of adsorption and photocatalytic reduction is weak. $TiO_2$ has high bandgap energy (3.2 eV) and thus it is used in limited visible light range, which deducts the efficiency of sun light for the effective applications of inorganic and organic contaminants degradation. The recombination of photogenerated electron and hole pairs leads to low performance of $TiO_2$ photocatalyst. Another material efficiently used in photocatalysis is ZnO nanoparticles [30]. The advantage of nanosize zinc oxide is environmentally stable, and low cost when compared with other nanoparticles metallic oxides. The main challenge of zinc oxide and titanium oxide is their high bandgap value, 3.2-3.3 eV [31]. To avoid these drawbacks, researchers have concentrated their studies on metallic oxides with other semiconductors. Effective separation

of charges can be obtained by coupling

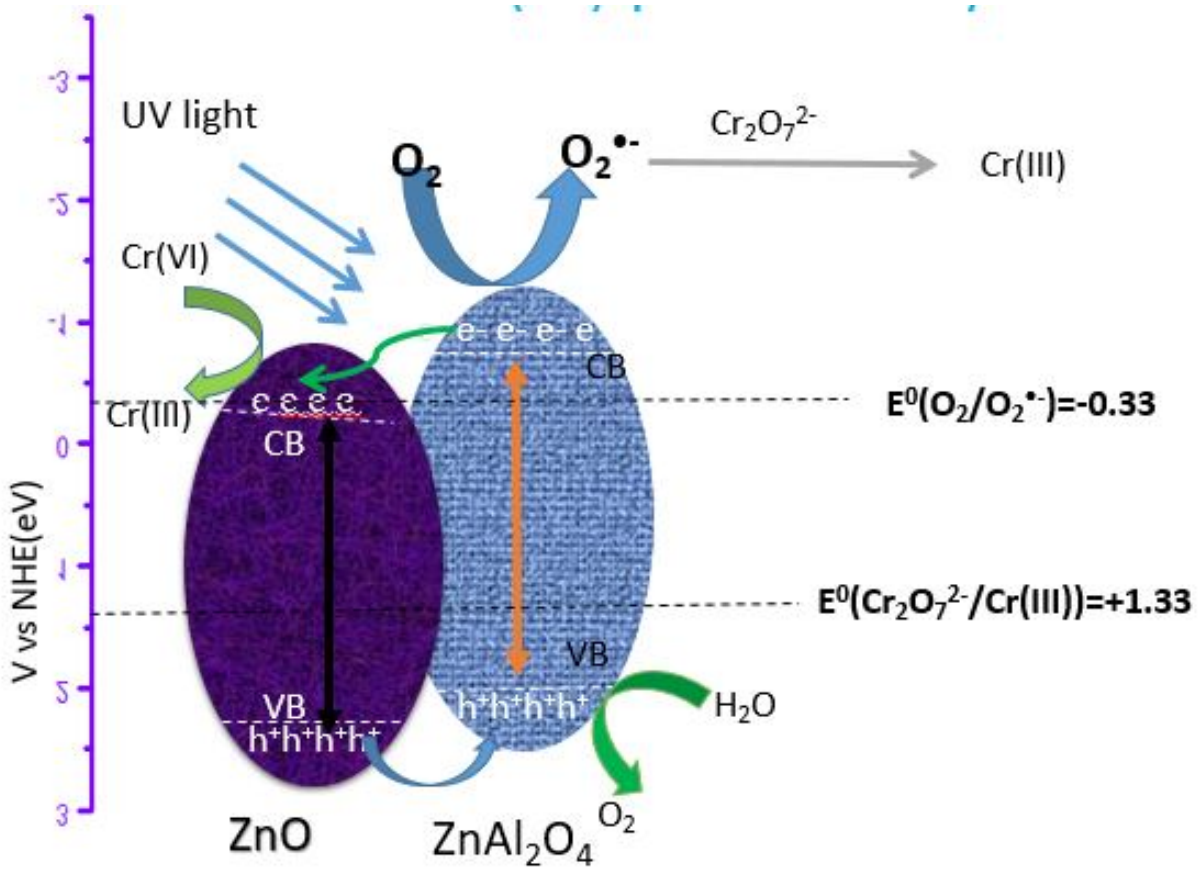


Figure 3. Schematic illustration of the mechanism of electron-hole separation and transport and Photocatalytic activity of ZnAl-MMO photocatalyst under UV light irradiation [32].

two or more semiconductor particles with different energy levels. Hence, it is necessary to combine with other semiconductor materials, such iodide [33, 34], nitrides [35], oxides [36], sulfides [37], to obtain photocatalytically active materials in visible light irradiation.

Among iodide semiconductors, AgI was reported for wastewater treatment in previous articles. In those articles, simultaneous photocatalyst oxidation and reduction enhancing technique over the 3D flower AgI/$BiVO_4$ p-n junction photocatalyst for both tetracycline (TC) oxidation and Cr(VI) reduction was reported. 0.3AgI/$BiVO_4$ is exhibited excellent photocatalyst activity [38]. Wang et al. (2016) confirmed that AgI/BiOI-$Bi_2O_3$ provided excellent photocatalytic performance under visible light irradiation for the reduction of Cr(VI) [39]. Wang et al. (2016) also reported AgI/$TiO_2$ photocatalytic reduction of Cr(VI) under visible light irradiation [40]. Vermurung s.et al. (2020)

used AgI-$Ag_2S$@g-$C_3N_4$ photocatalysts for efficient degradation of aqueous pollutants [41]. Yi Duan (2019) synthesized AgI/$Ag_3PO_4$ for the effective degradation of carbamazepine under visible light irradiation[42]. Moreover, porosity of the materials is also another important parameter to enhance the catalytic activity of the materials [43, 44]. Hence, it is important to use renewable biological resources to enhance porosity. Among biological resources, cellulose is the most abundant and can be used as a template [45]. So far, there is no report on cellulose templated Zn-Al LDH MMO combined with AgI semiconductor photocatalysts for effective removal of heavy metals.

In this work, we extracted cellulose from bagasse to make LDH porous after calcination which can enhance the catalytic efficiency. The calcination was changed the LDH into MMO and after dispersing into water. MMO has been re-generated due to memory effect [46]. Some of ZnO has been expected to form porous Zn-Al MMO; and certain ZnO combined with p-type AgI to enhance the catalytic activity. Hence, the Zn/Al layered double hydroxide with cellulose as a template was extracted from bagasse based MMO and combined with AgI nanocomposite. It is expected to be efficient for synergy adsorption and photocatalysis reduction of Cr(VI) solution.

## 1.2 Statement of the problem

Discharging of toxic chromium, Cr (VI), from industries is very dangerous for human beings and in general for living things. Several number of studies in the removal of Cr(VI) from wastewater were published. However, still it is a big question how to remove chromium efficiently from wastewater. Moreover, there was a question how to use a stable catalyst repeatedly. Hence, the Zn-Al layered double hydroxide based catalysts is important for efficient removal of heavy metals via adsorption or photocatalytic reduction under UV visible irradiation. Moreover, the porosity issue that used for the enhancement of photocatalyst performance needs modification by using cellulose, that extracted from sugarcane bagasse. Hence, bagasse was used as a template for the synthesis of porous LDH for effective removal of Cr(VI).

## 1.3 Significant of the study

In our research, we increased the efficiency of the LDHs and photocatalytic properties of the composite materials using visible light of solar energy to avoid hazardous Cr(VI) from wastewater. For instance, in our country electroplating plants do not have means of treating heavy metals and

dyes in plating plants. Those plants discharge the wastewater in to thank simple dilution with tape water. Still there is no any means to discharge into the environment due to lack of detoxification. So that this work may solve this type of problem with minimum cost and environmental friendly by the reduction of high toxic or harmful Cr(VI) pollutants in to non-toxic or harmless Cr(III) pollutants.

## 1.4 Objective of the study

### 1.4.1 General objective

Synthesis the environmental friendly cellulose templated LDH based MMO/AgI composites for effective synergy adsorption and reduction of Cr(VI) from wastewater.

### 1.4.2 Specific objectives

- To extract cellulose from sugarcane bagasse material that can be used for the cellulose templated Zn-Al LDH synthesis
- To optimize the ratio of synthesis LDHs and AgI with cellulose composites
- To check the effect of LDH calcinations for wastewater treatment
- Synergy adsorption and photocatalyst reduction performance evaluations of cellulose templated Zn-Al LDH based MMO/AgI composite materials with various amount ratio of AgI for the removal of Cr(VI)

## 1.5. Beneficiary of the study

The owners of electroplating plant, leather tanning industries and textile industries are basically the beneficiary of this study.

## 1.6 Scope of the study

The aim of this study was to synthesize calcined LDH and nanomaterial semiconductor composites with enhanced efficiency for photocatalyst reduction. Then various characterization was performed to identify and analyze by using synthetic chromium six pollutant. UV vis light was

used to optimize better photocatalyst composition ratio and reusability based on its degradation efficiency. Diffusiblity reflectance spectroscopy (DRS) was used to get the band gap of photocatalyst composite and identified the absorbance in various wavelength. X-ray diffraction test was also carried out to analysis the impurity of the catalyst with its diffraction peak 2θ angles position and measuring d-spacing between plane (hkl) $d_{hkl}$. The morphological analysis and composite component elements were detected by SEM and EDXS respectively.

# 2. Literature review

Water is the base of existence in alive and needs to be protected and preserved for future generation sake [47, 48]. World Health Organization (WHO) has predicted that most of the world population will not have safe water access in the future, and expected to increase lives in water shortage. Countries will cause additional problems of water pollution in the world [8].Water pollution faces a great problem nowadays since water ingredients a basic necessity in life and thus, is desired to all living things [49]. The highly rapid advancement of industries such as metal mining operations, paper, textile and fertilizers industries, leather tanning and pesticides have purposely discharged various types of wastes into the environment especially in developing countries [50]. Wastewater generates from water used in industries as impute for various activity that has a potential hazard for our environment because of introducing various contaminants such as heavy metals into soil and water resources. If there is no low cost, effective and efficient technology, wastewater can be reversed to the environment in different directions [51].

Industrialization and technological advancement have also placed an increasing risk on the environment by releasing high quantity of hazardous pollutants [52, 53]. Heavy metals (chromium, cadmium, and lead) and metalloids (such as antimony and arsenic, elements with properties between those of typical metals and non-metals), and organic pollutants that have created serious damage on the society and environment [4]. The deposition of heavy metals and metalloids in water continues to create severe health concerns. The accumulation of heavy metals in the environment can reach to caring organism through chemical chain elements seems like food chain, and thus may lead a significant health risk to caring organisms [54].

## 2.1 Wastewater

Wastewater is generated from served water resources like homes, private and public organization, urban areas, rural areas, industries, farms and others designated and non-designated sources [55]. Heavy metals Pollution of water environments is a worldwide environmental problem in the cause of their hazardous results and deposition through the food chain [56]. Heavy metals, phenols, dyes, pesticides, and inorganic anions (which are toxic to various living being forms and organisms) are available in the streams of wastewater discharged from several industrial processes. Printing, mining, dyeing, coating, electroplating, metallurgical engineering, nuclear power reactor,

aerospace, electronics and battery manufacturing processes are some of various types of pollutants that are generating in the industries wastewater effluents [57]. The discharge of unprocessed wastewater into the surrounding can lead to the pollutions of external water bodies like streams, rivers and lakes [58]. Industrial discharged water contains dangerous dissolved and undissolved particles, like heavy metals, and inorganic particles, when discharged without any treatment greatly affected the surrounding and causes sever health problems to living beings [7].

Urgent environmental concern of heavy metals are chromium , mercury, lead, cadmium, zinc, iron, and copper [59]. The expansions of industries mostly in developing countries like our country have attracted foreign investments but have led to heavy metal pollution of water contents due to the discharge of untreated industrial waste [50]. This pollution has been of great headache to governments and other concerned stakeholders. Therefore, searching treatment methods with affordable cost and effective result is the center of many researchers and scientists across the globe [28].

## 2.2 Toxic Heavy Metals

Heavy metals are the primary toxic chemicals that have specific gravity greater than 5 $g.cm^{-3}$ and five folds bigger than specific gravity of water at $4^{\circ C}$. In addition, heavy metals have high atomic number and atomic weight [60-62]. Heavy metal pollution is a quickly growing problem in streams, lakes, rivers, and oceans (water bodies). But relatively some type of heavy metals such as lead, cadmium, copper, zinc, cobalt, iron, vanadium, mercury, chromium, nickel, molybdenum, manganese, tin, and silver, in addition, the metalloids selenium and arsenic are related with the surrounding, plant, animal, or human health problems [63].

Even though the heavy metal chemical forms can be changed, they are not expose to chemical or biological destruction. Therefore, after discharge into the surrounding they are persistent pollutants [7, 64]. Natural phenomenon such as soil weathering, erosion of wind and water, volcanic eruption, spray of sea salt, and wild fires discharge heavy metals into the environment [4]. While the sources of anthropogenic discharges of heavy metals are lost in ancientness, they probably start as our prehistoric ancestors trained to extract metals such as copper, silver, gold, and tin from their derivatives and to make bronze [10]. The heavy metal pollution in the modern age has its starting with the revolution of industrial. The rapid advancement of industry, wide agriculture,

urbanization, and transportation over the past years, however, has been the essence of today's environmental pollution problems [65]. Anthropogenic exercise has also developed heavy metal dispersion by avoiding the materials from localized ore accumulates and moving them to other portion of the environment [66, 67]. The byproducts of heavy metal create from many processes including: extraction ore and smelting, fossil fuel burning, industrial wastes of dumping and landfilling, steel and iron making, cement and fertilizer manufacturing, wood combustion [68].

Water resources that are proximity factories and manufacturing industries may be exposed with heavy metals like mercury, copper, zinc, lead, nickel, cadmium, magnesium, iron and aluminum. If the metals transport to the sediment, they may transferred into the food chain via plants and under water animals [69]. The end result is heavy metal poisoning if the concentration in the water is above the required limit. In a global context, the main problem of surface water pollution is heavy metal discharge from industrial processes [4, 70]. In the developing continents like Africa development of industrialization is the primary source of heavy metals being discharged into aquatic environment, air and soil in worldwide, including Ethiopia. The main source of heavy metals are mostly industries [58, 71, 72]; industries like electroplating, metal and mining, chemical and petrochemical, leather, ceramic, textile, fertilizer, cement, tanneries, batteries, paper, pesticides and others [73]. These industries discharge their wastewater consisting different hazardous heavy metals without treatment into the surroundings [74]. These harmful toxic chemicals elements consist such as uranium (Ur) [75], selenium (Se) [76], zinc (Zn) [77], silver (Ag), gold (Au), nickel (Ni), cadmium (Cd), mercury (Hg) [78], copper (Cu) [79, 80], chromium (Cr) [81], arsenic (As) [82], lead (Pb) [77] and others. The existence of these toxic heavy metal elements, even at low concentrations, affects the health of humans and other living beings [83]. The fact that these elements are highly soluble in water and exist for a long period of time in the soil, makes their presence in water bodies are more dangerous [84].

## 2.3 Effect of Heavy metals on human health

Excess amount of heavy metals in the surrounding are hazardous to the health of human beings and other living organisms [85]. The gradual deposition of toxic chemicals in the body of a living beings can result accumulation in the organ of human body [86]. Accumulation in the body happens when an organism uses toxic substance more than its avoid ability [87]. Therefore, the higher deposited of these chemicals in the body of human being is larger than their release ability

may occur gradually [88]. As these components cannot decompose or break down easily, the consequences are worsened by the ecosystem of the environment [89]. For instance, Cd can be stored in the human body for a years, without being decomposed or becoming soluble like organic matter[90]. According to the study untreated industrial wastewater containing heavy metals (Pb, Cd, Hg, Zn, Cr, As and Fe) discharged into non polluted aquatic bodies can also be deposited in the bodies of aquatic organisms [7]. Therefore, the requirement to treat polluted water is great importance in order to protect the environment and deduct related health problems [91]. The greatest concern with regard to human health are heavy metals which are Pb, Hg, Cd, Cr, and As hazardous even at trace level. Most products such as some drugs, and Unani drugs, pharmaceutical products and dental products, cosmetic products and others contain heavy metals [92]. Hexavalent chromium (Cr(VI)) is one of the most common pollutant among the hazardous heavy metals from industrial wastewater including leather tanning, pigment production, textile manufacturing, electroplating depositing and so on [93].The metals are transferred from these materials by the means of food chain or food web and by coming in contact with the skin from the surround to humans and other living organisms. In the food chain process, heavy metals are absorbed into the body of the organism through taking food that consists high amount of heavy metals, or by drinking water, breathing air, contact with skin and eye and other sense organs [94]. Small amounts of these elements, beyond allowable limits, have strict results and are unsuitable for living organisms because of their high energy particle output [95]. Due to this, wellbeing of living organisms' is compromised and living organisms are easily exposed to different diseases and associated problems such as carcinogens, mental disorders, lung fibrosis, kidney damage, high blood pressure, liver disease, intestinal problems, headaches, anxiety, depression, reduced cognitive, panic disorder and response capacity, Parkinson's disease, although not as consistently, with Alzheimer's disease and others [96, 97]. Therefore, it is important to eliminate heavy metals from contaminated water to avoid point and non-point problems.

## 2.4 Methods of Wastewater treatment

Photocatalyst is the method of purifying wastewater. This operation is highly important due to the fact that some contaminants or pollutants are difficult to control after discharge from source pollution to surroundings [98]. Wastewater treatment in conventional way is divided into three stages; primary, secondary and tertiary. Screening, grit and primary purification are used to avoid

the large particle materials and sands. Biological treatment, belongs to secondary treatment, uses microorganisms to degrade the contaminants. The treated water obtained from secondary treatment transformed tertiary treatment may undergo coagulation, sedimentation, filtration, and disinfection when reuse or recycling is necessary for the aim of the discharge water [99]. These stages depend on type of discharge wastewater, the amount of harmfulness, and cost effectiveness. Making polluted water functional for consumption and use again is not an easy process. No one purification or filtration method works for all types of water pollution [100]. Recycle wastewater to use again after pollution, must be treated with a variety of filtration and purification methods. Therefore, it is important to treat heavy metals discharge from industrial wastewater, with affordable and technically feasible methods. This initiates the need for exploring cost-effective, simple and efficient removal techniques [10].

The choice of a desirable wastewater treatment technology (WWTT) is a complex operation because it needs long experience, expertise, and feasibility studies. Conventionally, this selection has been based on technological and economic factors. However, social, regulatory, governmental, and environmental factors also need to be counted along with technological and economic factors for decision-making [101].

## 2.5 Methods of heavy metals removal

Water is often happened with high concentration pollutants that could be in solution or dispersed as insoluble phases frequently forming emulsions and colloids. Among pollutants happened in fresh water are organics and heavy metals. These materials are difficult to process frequently because to the tremendous amounts of water that is produced by urban and industrial processes; therefore, the ideal process to clean polluted water should be operating in a continuous way to minimize fixed and operating costs.

Heavy-metal ions are naturally toxic. Thus, polluted water mixed with poisonous metal ions are being discharged into the surrounding, crating threat on human health and ecosystems. Therefore, water treatment methods with low price and high efficiency must be developed. Methods of treating wastewater presently include chemical photocatalysis, precipitation, chemical coagulation, biodegradation, ion exchange and adsorption [5, 44, 71].

### 2.5.1 Chemical precipitation

Chemical precipitation, formation of a solid particle from a chemical solution, either by changing the substance into an insoluble form or by converting the compositions of the solvent to lower the solubility of the substance in it [102]. The difference between precipitation and crystallization lies highly in whether emphasis is placed on the process by which the solubility is reduced or on that by which the construction of the solid substance becomes organized [103]. Chemical precipitation is the highly usable technology needed in avoiding dissolved (ionic) metals from solutions, such as process wastewaters containing toxic metals. The ionic metals are changed to an insoluble form or particles by the chemical reaction between the soluble metal compositions and the precipitating reagent. The particles formed by this reaction are removed from solution by decanting and/or filtration. The unit operations especially needed in this technology include precipitation, neutralization, solids/liquid separation, coagulation/flocculation, and dewatering [104].

The effectiveness of a chemical precipitation process is dependent on several factors, including the type and concentration of ionic metals present in solution, the precipitate used, the reaction conditions (especially the pH of the solution), and the presence of other constituents that may inhibit the precipitation reaction [105]. Hydroxide precipitation (also referred to as precipitation by pH), is the most widely used chemical precipitation process in which metal hydroxides are formed by using calcium hydroxide (lime) or sodium hydroxide (caustic) as the precipitant [106]. Each dissolved metal has a different pH value at which the optimum hydroxide precipitation occurs from 7.5 for chromium to 11.0 for cadmium. Metal hydroxides are amphoteric, which means that they are increasingly soluble at both low and high pH values. Therefore, the optimum pH for precipitation of one metal may cause another metal to solubilize or start to go back into solution [107].

### 2.5.2 Ion exchange

Ion exchange materials are insoluble substances containing loosely held ions which are able to be exchanged with other ions in solutions which come in contact with them. These exchanges take place without any physical alteration to the ion exchange material [108]. Ion exchangers are insoluble acids or bases which have salts, and this enables them to exchange either positively

charged ions (cation exchangers) or negatively charged ones (anion exchangers) [109]. Many natural occurring such as cellulose, proteins, living cells and soil particles display ion exchange properties which play an important role in the way of the function in nature. The process of ion exchange is one of the most utilized techniques in water and water treatment as well as in breakup processes as synthesis of chemical, food processing, medical research, mining, agriculture, etc. [110]. The way of ion interchange is followed by an irreversible response in the resin phase namely:

$$R{-}2Na^{+} + Pb^{2+} \leftrightarrow R{-}Pb + 2Na^{+} \text{----------(1)}$$

where R is the resin origin part

In water purification the aim is usually either to soften the water or to remove the unwanted mineral content altogether. The water is softened by using a resin containing $Na^{+}$ cations but which binds together with $Ca^{2+}$ and $Mg^{2+}$ more strongly than $Na^{+}$ independently. As the water passes through the resin the resin takes up $Ca^{2+}$ and $Mg^{2+}$ and releases $Na^{+}$ making for a 'softer' water [111]. If the water needs to have the mineral content entirely removed it is passed through a resin consisting $H^{+}$ (which remove all the positive ions) and then through a second resin consisting $OH^{-}$ (which remove all the negative ions). The $H^{+}$ and $OH^{-}$ then respond together to offer more water [108].

Ion exchange is needed as one of the heavy metals avoiding processes. This process appears to be efficient to remove different kinds of heavy metals and the ion exchange resin can be easily regained and reserved by re-formation functioning. Ion exchange is the process through which ions in solution are changed to a solid matrix which, in turn discharge ions of a various type but of the same charge[112]. The main application of ion exchanges is regaining of metal value, preferentially, small sludge amount created and the obtaining of accurate discharge specifications. Different types of exchange materials, which are differentiated into natural or synthetic resins, are available in a market. Besides, the competition effect between a small amount of heavy metal ions and a large amount of salts often causes to a substantial decline in heavy metal avoidance using ion exchange part[113]. Ion exchange using solid adsorbents have been a predicting methods for treating wastewater, owing to its importance such as operating simplicity, minimum cost,

availability in large amount and ability to treat pollutants in a sufficiently large scale operation [114].

### 2.5.3 Electrolysis

Electrolysis, process by which electric current is applied through an electrolyte solution to result a chemical change, i.e. ions separation. The substance loses or gains an electron (oxidation or reduction) is occurred due to the chemical change. The action is performed in an electrolytic cell, the parts containing of positive and negative electrodes held individually and immersed into a solution consisting positively and negatively charged ions [115]. Electrolysis is less applied or less popular for water treatment, as power was the main requirement and also expensive in the previous decades in the world and electrode materials were another headache [116].

### 2.5.4 Membrane filtration

A membrane is a semi-permeable thin layer of material which has a capability of separating pollutants as a function of their physical/chemical properties. It is a thin layer of material that will only permit certain compounds to pass through it [117]. The membrane size and the chemical characteristics is determined which material will pass through the membrane and which material remains [5]. A membrane can separate substances when a driving force is applied across the membrane. Membrane processes are highly used for removal of bacteria, microorganisms, particulates, and natural organic material. Different membrane processes are microfiltration (MF), ultrafiltration (UF), nanofiltration (NF), and reverse osmosis (RO) [118, 119].

### 2.5.5 Coagulation-flocculation

Surface water consist both dissolved and suspended particles. Coagulation and flocculation are used to differentiate the suspended solids parts from the water. Suspended particles vary in origin, charge, size, shape, and density [120]. The right application of coagulation and flocculation depends upon these factors. Suspended solids particles in water have a negative ion and since they have similar type of surface charge, they repel each other when they come near each other [121]. Therefore, suspended solid particles will remain in suspension and will not join each other and settle out of the water, unless desire coagulation and flocculation is used [122]. Coagulation and flocculation occurs in frequent steps, providing particle collision and growth of floccule. This is

then next to sedimentation. If coagulation is incomplete, flocculation step will be unsuccessful, and if flocculation is incomplete, sedimentation will be unsuccessful [123, 124].

#### 2.5.5.1 Coagulation

Coagulant chemicals with charges opposite those of the suspended solids are added to the water to neutralize the negative charges on non-settlable solids (such as clay and color-producing organic substances). Once the charge is neutralized, the small suspended particles are capable of binding together [125]. Then slightly create larger particles known as microflocs, and are not visible to the human eye. Water surrounding due to the newly formed microflocs should be clear. If not, more coagulant chemicals may need to be added to remove the remaining charged particles [126]. Contact time in a high-energy rapid-mix chamber is typically 1 to 3 minutes, for the proper disperse coagulant and promote particle collisions [127].

#### 2.5.5.2 Flocculation

Flocculation, a gentle mixing step, develops the particle size from invisible microfloc to visible suspended particles. Particles collision causing them to bond to produce larger, visible flocs known as pinflocs [128]. Addition of inorganic polymers (coagulant) or organic polymers increase the size of floc with additional collision and interaction. Once floc has reached it optimum size and strength, water is ready for sedimentation. Require contact length for flocculation ranges from 20 minutes to an hour or more [129, 130].

### 2.5.6 Floatation

Flotation can be explained as a gravity isolation process, in which gas bubbles contact to solid particles to cause the apparent density of the bubble-solid aggregates to be less than that of the water thereby allowing the aggregates to float to the top surface [120]. The various methods of generating the gas bubbles give rise to various types of flotation processes which are electrolytic flotation, dispersed-air flotation and dissolved-air flotation [131].

### 2.5.7 Adsorption

Adsorption is the capability of all solid particles to attract to their bodies molecules of gases or solutions with which they are in contact. Solid particles that are needed to adsorb gases or dissolved

substances are known as adsorbents; the adsorbed molecules are usually cited to generally as the adsorbate [132]. For good example charcoal used as in gas masks to eliminate impurities or poisons from a flow of air. Adsorption indicates the molecules accumulating by the external or internal bodies (walls of capillaries or crevices) of solid particles or by the surface of liquids[133]. Absorption shows to processes in which a substance immobilized into the internal part of solid particle, of none-crystalline solids, or of liquids [134]. Sometimes the word sorption is used to indicate whether the process is adsorption or absorption. Adsorption could be either physical or chemical in nature [117]. Physical adsorption relates the change of+ gases to liquids by condensation based on the physical, or van der Waals, force of attraction between the solid particle adsorbent and the adsorbate molecules [15]. Chemical adsorption occurs mostly at higher temperatures than those at which physical adsorption occurs; furthermore, chemical adsorption is commonly a slower process and requires activation energy unlike physical adsorption. Traditional physical adsorption methods can efficiently adsorb contaminants, but can't completely remove the contaminants [81].

### 2.5.8 Photocatalyst reduction

The development of high efficiency, green energy sources and eco-friendly methods for environmental remediation and energy generation has become an imperative task. As a new and effective green technology, photocatalytic technology can utilize sunlight to effectively remove toxic and harmful organic pollutants in the environment [52]. Photocatalysts are the core of photocatalytic technology. However, traditional photocatalysts that are one of the earliest studied photocatalysts can only utilize ultraviolet [135]. Photocatalytic technology has advanced into a hopeful technology for environmental rehabilitation due to its low toxicity, high output and low cost [136]. Therefore, the advancement of green and effective wastewater treatment technology has become a great issue. Semiconductor photocatalysis, known as “green chemistry process”, has been payed high interest. Semiconductor photocatalysis technology owns some distinct importance, for example modest reaction conditions, no secondary pollution and high output to impute ratio, and it can provide the interactive reaction between some pollutants to simultaneously remove a variety of pollutants, such as the interactive removal between Cr(VI) and organic pollutants [81].

The efficiency of the photocatalytic is still inadequate due to the severe recombination or/and unsatisfactory reduction-oxidation potentials of photo emitted charge carriers in a most of photocatalysts. To break through these drawbacks, different ways have been advised to enhance the separation efficiency of the photo emitted electrons and holes in photocatalysts [137]. Production of heterostructure photocatalysts by coupling different semiconductors having matchable band structures is an effective approach to avoid the charge recombination by spatial separation of photo-generated holes and electrons [138].

### 2.5.9 Heterogeneous photocatalysts

The huge lion-share of energy on earth is gained from solar energy, but it cannot be utilized directly, and must be captured and changed into an appropriate form of energy resource. In order to make effective application of solar energy, two limitations should be avoided: find out how to convert solar energy into a functional form and search the setup of the light-harvesting complex [139]. The photosynthesis of nature plants gives a good source for researchers, which sunlight is initially absorbed by chloroplast consisting chromophores, followed by energy changer to devoted reaction center, and finally the stored energy is changed into chemical energy. The green plant leaves with porous structures and functional components have a high energy collecting area and can advance the light collecting property [140]. Photovoltaic cells with great light obtaining area are one of the main requirements for the solar energy application. They can condense small solar energy into electrical energy, which is an easy-to-use form of energy. Therefore, it is highly desired to design a system that simulates the energy conversion and structural properties of the green leaves, which can effectively convert sunlight into other energy that can be utilized [141].

For emerged technologies used to treat water, heterogeneous photocatalysis gives high performance under updated physicochemical processes. Thus, it is recognized as an advancing technology for water purification at present [142]. Among the different photocatalytic systems, the semiconductor heterogeneous photocatalyst has considered excellent candidate for photocatalytic absorption bodies of visible light/solar spectrum, less recombination rate, well redox ability. Due to energy position variation of semiconductor based material of the valence band (VB) and conduction band (CB)is greater than that of other material, the band-position lays in between these two materials drive the electrons flow to one semiconductor and holes to the other. Therefore, energy band gap effect decreases the range of recombination of photo generated electron/hole pairs

[143]. Many studies have shown that the close interface between the noble metal nanoparticle and semiconductor photocatalyst is very advantageous to obtain the require separation and transportation of photo-generated carriers. In order to enhance the photocatalytic performance decreasing the recombination rate of charge-carriers and stimulating the process of charge transfer is required during the production of homogenous photocatalyst [144].

For the complete separation of electron hole pair in a heterogeneous photocatalysis, the metal nanoparticles are used as co-catalysts that enhance electronic transport rate because of the fact that metal nanoparticles are better sink for electrons leaving behind hole that in search of electron generates more electrons and hence increases the charge separation rate for enhanced photocatalytic activity [145].Many recent studies have indicated that through production process heterojunction structure using two different semiconductors, advanced electron/hole separation efficiency and improved redox ability of the photocatalyst can be obtained [146].

## 2.6 Layered double hydroxide (LDH)

Layered double hydroxides (LDHs) are one of layered materials whose arrangement is consisted of brucite ($Mg(OH_2)$) like layers joined with interlayer anion. Mg cations contain the center of the octahedron, which have hydroxyls in the edges [147]. A part of the divalent cations in the brucite like sheet are substituted by trivalent ions, giving positively charged outer layers, and for the electroneutrality of the positive charge, anions occupy the interlayer space as shown in Figure 4. The chemical formula of LDH is explained as $[M^{2+}_{1-x}M^{3+}_{x}(OH)_2]^{x+}(An^{-})_{x/n}\cdot yH_2O$, where $M^{2+}$ and $M^{3+}$ are divalent (e.g., $Mg^{2+}$, $Ni^{2+}$, $Zn^{2+}$, $Cu^{2+}$) and trivalent (e.g., $Al^{3+}$, $Fe^{3+}$, $Ga^{3+}$) metal cations in the sheet, respectively, x is the ratio of $M^{3+}/(M^{2+} + M^{3+})$, and $A^{n-}$ is the interlayer anion ($CO_3^{2-}$, $NO_3^-$,$Cl^-$). The interchangeabilities of the chemical component (combination of different $M^{2+}$ and $M^{3+}$) make LDHs useful for versatile applications [148].

In this case, the lamellae are not only joined by hydrogen bonds, as in the case of the brucite, but also by electrostatic attractions between the positively charged plates and interlayer anions.

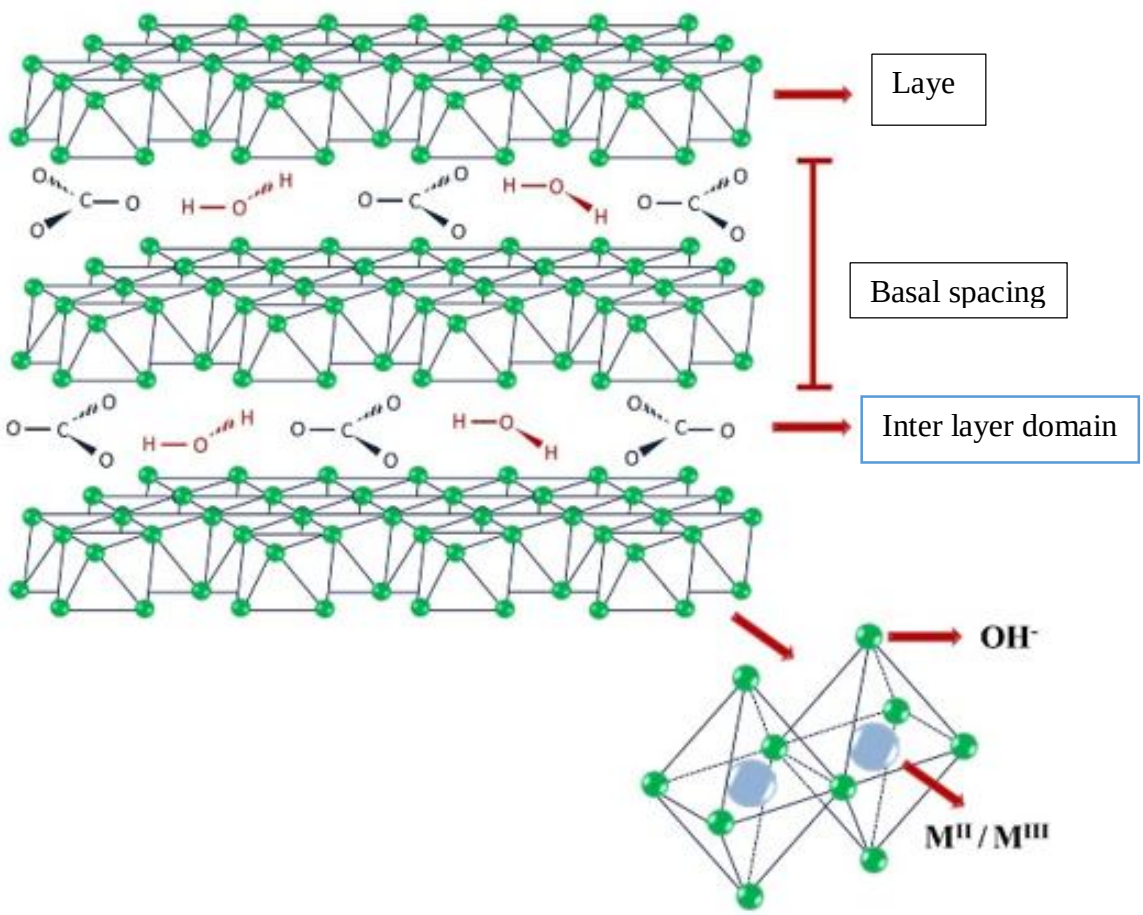


Figure 4. Layered Double Hydroxides (LDH) structure scheme [20].

In the last few years, the layered double hydroxide materials (LDH) have brought up great attentions due to their special properties, such as lamellar structure, high surface area, acidic-basic buffering capacity, high ion-exchange capacity, economic and the versatile. These materials have great potential applications in different fields [149]. LDHs are thought to be more efficient as visible light activated photocatalysts application, owing to their versatility in composition, morphology and construction, as well as their special structural properties (intercalation, topological transformation, catalyst support and self-assembly with other functional materials) [150]

## 2.7 Methods for Synthesis of photoactive LDH

### 2.7.1 Co-precipitation method.

The method of coprecipitation is the widely used preparation method for LDHs[151]. It has been applied extensively for the one-pot direct synthesis of LDHs consisting different layer of cations and interlayer anions[152]. It also promising to scaling up in order to produce high amount of material. In the coprecipitation process, aqueous solutions of $M^{2+}$ and $M^{3+}$consisting the anion that is to be merged into the LDH are needed as precursors. Of the different (M(2)/M(3)) ratio LDH systems, shows a variable composition, while certain phases can be gained only within a small range of ratios [103]. This variability in the layer charge density permits the packing density of the interlamellar anion to be different. Another attracting feature of this preparation way is that a different variety of anionic species can be directly intercalated between the hydroxylated sheets. This synthesis method is often the method of choice for the preparative of organic anion-consisting LDHs which are not gain in other means. In order to confirm simultaneous precipitation of two or more cations, it is necessary to perform the synthesis under super saturation conditions [106]. Generally, super saturation conditions are obtained by managing the pH of the solution. In particular, it is necessary to precipitate at a pH more than or equal to the one at which the high soluble hydroxide is precipitated. Next to coprecipitation, a thermal treatment is often carried out in order to enhance yields and/or the crystallinity of non-crystalline or badly crystallized materials [153].

### 2.7.2 Hydrothermal method

Hydrothermal process is the frequently common method and cheap to make semiconductors/LDHs nanocomposites [154]. This is very simple and realistic process for production of semiconductors/LDHs photocatalysts by hydrothermal way which high purity sample may be achieved [155]. The synthesized clear suspension was transferred to the Teflon lined stainless steel autoclave at controlled temperature and time accordingly , the solid result was obtained by centrifugation and washed with distilled water and ethanol many times and dried at room temperature [20].

### 2.7.3 Sol-gel method

Sol-gel method gives a novel process to the manufacturing of new nanomaterials. Sol-gel method is one of the well-established production processes to synthesize novel metal oxide nanoparticles as well as to LDH based mixed oxide materials. This technique has continuous manage over the textural and surface characteristics of the components. Not only, high purity and homogeneity of sol–gel way is frequently used to build LDHs and its composites. For instance, synthesized MgAl LDHs/$TiO_2$ composite by sol gel process for degradation of phenol as model organic dye in aqueous solution [26].

## 2. 8 Photocatalytic activities of LDH based MMO

MMOs can be produced by calcination of LDHs. Mixed metal oxides are highly performed in heterogeneous catalysis [156]. It has been indicated that transition of crystal facets and external defect structures of metal oxides can have a significant influence on their catalytic efficiency. In this respect, MMOs gives considerable advantages, since the exposure of crystal facets and defect structure can be controlled by differing the method of transformation parameters (e.g., heating rate, calcination temperature, and calcination atmosphere) of the LDH precursors [157]. Upon calcination, LDHs can be changed into hetero-structured mixtures of mixed metal oxides (MMOs) with necessary properties in aqueous medium, thermal and structural performability, high surface area and good hetero-metallic distribution [158]

## 2.9 LDH based MMO and composites

It is well known that calcination can change the LDHs to the mixed metal oxide (MMO) structures. The MMOs are consisted of equally dispersed elements, which have low bandgap energies, high surface area, better thermal and chemical stability than the LDHs. Therefore, LDHs is used a desirable way for preparation of the highly distributed metal mixed oxides with good photocatalytic efficiency. A favorable approach to increase the photocatalytic activity, the result gives especial properties, such as high quality, low resistivity, strong UV emission, and high transparency to visible light [150]

After calcinations, LDHs is changed into non-crystalline mixed metal oxides (MMOs). Mixed metal oxides obtained in this way show a very uniform sharing of the various cations within the

mixed oxide structure, which is a conceive cause for use of the layered double hydroxides as a source for MMOs catalysts and catalyst supports [159]. Moreover, it is remarkable that many LDHs modifications expose the special characteristic termed as the “memory effect” after calcinations up to a certain temperature it is possible to regain the LDH structure with rehydration or aqueous solutions of certain lost or required intercalate anions. The LDH with excellent dispersion of metal cations and high surface area perform as good catalysts for various chemical reactions [20].The mixed metal oxides(MMOs) photocatalysts, which coupled with two or more metal oxides, are separate photo-induced electron-hole pairs through properly arranging the band structures, and then enhance the lifetime of electrons and holes in comparison with common photocatalysts (such as ZnO or $TiO_2$) [22]. Fabrication of a $ZnO/ZnAl_2O_4$ heterogeneous structure by appropriate thermal treatment of the ZnAl LDH precursor, which gives excellent separation efficiency of photo-generated charge carriers [157].

## 2.10 Silver iodide composite

Silver halides, including AgBr, AgI, and AgCl, which are the same source materials in photographic film, have been newly needed as photocatalysts [160]. Among them, AgI is a moderate band gap energy (2.80 eV) material, has presented excellent ability for photocatalytic degradation of many different organic pollutants even applied by visible irradiation. AgI is also needed to adapt with other photocatalysts to improve their charge carrier separation and light absorption efficiency. Meanwhile, in cause of high conduction band potential (0.4 eV), AgI has been taken as matching material for construction of Z scheme heterojunction system [30]. As a consequence, different AgI based Z scheme heterojunction systems, such as $AgI/TO_2$ [36], AgI/N-$TiO_2$ [161], $AgI/Ag_6Si_2O_7$ [162], $AgI/BiVO_4$ [163], $AgI/BiVO_4$ [164], have been manufactured and applied in photocatalytic contaminants decomposition and energy conversion over the last years. Currently, Ag-based semiconductors have described increasing requirements in photocatalysis area, due to their excellent efficiency in photocatalytic decomposition of organic pollutants and disinfection [165].

## 2.11 Cellulose template photocatalysts

Cellulose is the first most abundant biopolymer on earth. It is natural, renewable, environmental friendly, cost effective, nontoxic, bio-degradable and bio-compatible. It is derived from plant

sources such as grasses, reeds, stalks and woody parts. It consists of over ten thousand repeating units of β-(1→4)-D-glucose linkage and has the formula $(C_6H_{10}O_5)_n$ [166].

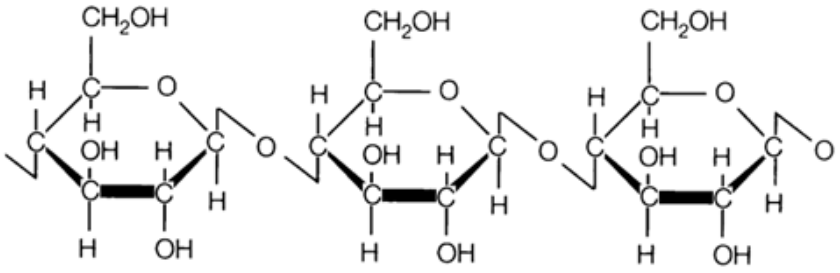

Figure 5 Structure of Cellulose

Particularly, sugarcane bagasse is a by-product of agricultural wastes that consists of cellulose (50%), hemicelluloses (27%) and lignin (23%). The cellulose from sugarcane bagasse can be obtained by acid hydrolysis through the use of sulfuric acid after bleaching the sugarcane bagasse with sodium chloride and glacial acetic acid [167]. Cellulose uses for the preparation of nanoparticles on cellulose matrix with the aim of to improve the adsorption and photocatalytic activities of metallic oxide [168]. Many researches have indicated that the materials prepared by the bio-template process exhibit a hierarchical porous structure and a high surface area. Bio-template technology is now accepted as a minimum cost and ecofriendly way to produce different materials with identical structures and necessary properties [169].

## 2.12 Influence of pH

The $Cr^{6+}$ are soluble in water and highly toxic. Under toxic conditions, chromium can exist as bi-chromate ($HCr_2O_4^-$) or chromate ($Cr_2O_4^{2-}$), depending on the pH of the aqueous system. These oxy-anions are readily reduced to trivalent forms when the electron donors (reducing reagents) exist in aqueous solution. The reduction rate increases as the pH decreases. Trivalent chromium ($Cr^{3+}$) species are very stable with respect to the oxidation reduction potential. They can react with particulates and form metal salts as $Cr(OH)_3$ that are less soluble in water when the pH is 8–10 or higher [117, 134].

# 3. Research Materials and Methodology

## 3.1 Chemicals and Reagents

All chemicals and reagents used in this study were analytical grades and used as obtained without any further purification. Zinc (II) nitrate hexhydrate ($Zn(NO_3)_2.6H_2O$) (Uni-Chem), aluminum (III)Nonahydrate (99.9%, $Al(NO_3)_3.9H_2O$) (Avi- chem, India), silver nitrate ($AgNO_3$), potassium iodide (KI), Sodium hydroxide (NaOH 99.8) (Ranckem, Turkey), sodium Carbonate ($Na_2CO_3$) (Alpha chemika, India), potassium dichromate (99.9% $K_2Cr_2O_7$) (LOBA CHEMIE PVT. LTD), hydrochloric acid (HCl), hydrogen per oxide ($H_2O_2$), sulfuric acid ($H_2SO_4$) (LOBA CHEMIE), acetic acid($CH_3COOH$) (Abron Chemicals, India), sodium hypochlorite (NaClO), 1,5 diphenylecarbazide (DPC) (Nice India), Acton ($C_3H_8O$) (chung chun plastic co.Ltd), and ethanol were used in our experiment. Distilled water was also used throughout the experiment.

## 3.2 Cellulose extraction from sugarcane bagasse

The sugarcane bagasse was collected from Wonji sugar factory. Then, the sugar cane bagasse (SCB) was washed with distilled water several times until the foreign materials washed away. Next

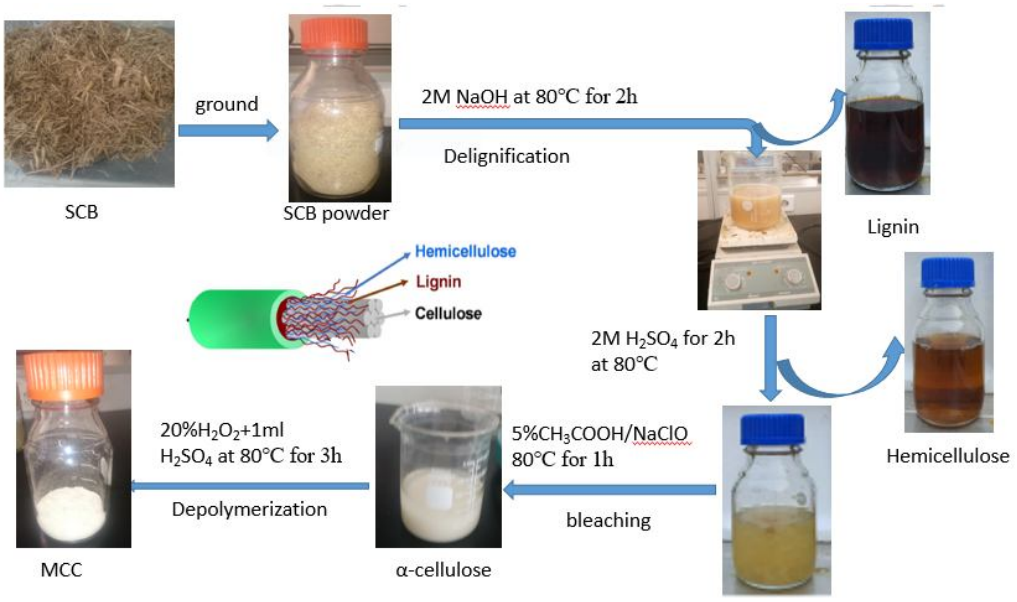


Figure 6. Cellulose extraction processes from sugarcane bagasse

the SCB was filtered to remove the excess water and dried outdoor sun light up to the weight become constant. The dried SCB pound by mortar for size reduction and ground by grinding machine for further size refinement approximately a fraction of millimeters. Grounded SCB was first treated with 2 M NaOH at 80℃ for 2 h with continuous stirring for the removal of lignin and diluted with distilled water. Then, 0.5 M $H_2SO_4$ used to treat the SCB further at $80^0$C for 2 h with stirring and diluted with distilled water. The residue was then dried and bleached with 5% acetic acid to sodium hypoclorate ($CH_3COOH/NaClO$) at 80℃ for an hour. Depolymerization was performed with 20% $H_2O_2$ and 1 mL of $H_2SO_4$ at 80℃ for 3 h. The resulting bleached sample was dried and then grounded to produce a white, crystalline powder of SCB.

### 3.3 Synthesis Zn-Al LDH

The Zn-Al LDH was prepared by using co-precipitation method. In a particular procedure, a 0.9 mol/L of $Zn(NO_3)_2.6H_2O$ and 0.3 mol/L of $Al(NO_3)_3.9H_2O$ salts were added into aqueous solution (150 mL) with a molar ratio Zn/Al 3:1 and assigned as solution A. Another solution consisting of 2 mol/L NaOH and 0.6 mol/L $NaCO_3$ was simultaneously added into 100 mL deionized water and assigned as Solution B. Then, solution B was added into aqueous solution of solution A with vigorous mechanical stirring. The pH of the mixed solution was controlled at about 10. Then, resulting slurry was aged at 70℃ for 24 h and washed several times with distilled water until the pH of the mixture become 7. After centrifugation and drying at 60℃ in an oven, all samples were ground in a mortar, sieved to separate large particles with 100 mesh size sieve. Then, the powders were calcined at 500, 700, 900 and 950℃ temperature.

### 3.4 Synthesis cellulose-templated Zn-Al LDH

The required amount of SCB extracted cellulose was socked in de-ionized water (40 mL) at 60 ℃ for 30 min in a beaker. Then, zinc nitrate and aluminum solution (150 mL) 3:1 molar ratio was added into a beaker containing dropwise and stirring with magnetic stirrer and assigned as solution A. Another solution consisting of 2 M NaOH and 0.6 M $NaCO_3$ was simultaneously added into 100 mL deionized water and assigned as Solution B. Then, solution B was added into aqueous solution of solution A with vigorous mechanical stirring. The pH was adjusted with NaOH to maintain pH 9.5-10.5. Then, precipitate mass was aged for 24 h under the same conditions, filtered,

washed with distilled water till the solution become pH=7 and dried at 60 ℃ under static air. The obtained solid was grind with a grinder and the cellulose template Zn-Al LDH was calcined with 500,700, 900 and 950℃ temperature to remove cellulose.

**3.5 Synthesis cellulose-templated Zn/Al MMO /AgI**

A 0.5 gm of the cellulose template Zn/Al MMO powder and various amount of KI was added in to 60 mL of distilled water and stirred for 30 min for uniform distribution and refluxing. Then, the solution was sonicated with ultra-cleaner sonicater. Then, various amount of $AgNO_3$ was prepared with 30 mL of distilled water. After 30 min sonication of the first solution, $AgNO_3$ solution was added drop by drop with vigorously stirring. The yellow suspension was obtained that indicates the AgI formation. After addition of $AgNO_3$ the solution was further sonicated for 1 h. After reaction, the solution was washed with distilled water several times, and dried at 100 $^0$C. The obtained ZnO/$ZnAl_2O_4$/AgI was annealed for 2 h at 350℃. This composite was prepared by varying the weight percent of AgI 10, 20, 30, 40 and 50% that of ZnO/$ZnAl_2O_4$.

## 3.6 Characterization of photocatalyst

The XRD measurements of photocatalysts ZnAl-LDH, ZnAl-MMO and MMO-AgI composites were carried out at room temperature on an x-ray Powder diffraction method, with the Bragg–Brentano geometry, using CuKα target (λ = 0.15406 nm) operated at 40 KV and 30 mA. Scherrer Eq. was used for calculating the average crystal size of particles:

$$D = \left[\frac{k\lambda}{\beta \cos\theta}\right] \text{----------(2)}$$

where D =average size of the crystals; k = shape-dependent Scherrer's constant (0.90); λ=radiation wavelength (0.15406 nm); β = full width at half maximum intensity (FWHM given in radians); θ=Braggs diffraction angle.

The texture and surface morphology of C-ZnAl-LDH, C-ZnAl-MMO and C-ZnAl-MMO-AgI were determined using a Field Emission Scanning Electron Microscope at an accelerating voltage of 10 kV. The SEM images were obtained at a magnification of 5 kxHV. The elemental composition of the samples was obtained using Energy Dispersive X-ray Spectrometer in conjunction with SEM.

### 3.7 Photocatalyst reduction

Photocatalytic reduction experiments were carried out by using 100 mL of 20 ppm Cr(VI) ions solution and 40 mg photocatalyst in aqueous solution. The solution was sonicated for 30 min with ultra-sonicate cleaner bath for the adsorption desorption equilibrium. After ultra-sonication, the suspension was illuminated under visible light source with stirring. The sample of the solution was taken in every 15 min interval for 90 min. The Cr(VI) ions concentration in the supernatant liquid was determined with spectrophotometrically following a standard procedure at 542.5 nm wavelength. The concentration of Cr(VI) was also determined using standard 1,5 dyphenylcarbazide and sulfuric acid for the complexing agent of Cr(VI) by adding 3 drop each on 3 mL suspension. Moreover, the pH effect also evaluated on the reduction [19].

In order to study the stability of the photocatalyst during the reaction, each degradation cycle listed, and the used photocatalyst was collected and used to repeat the same degradation experiment cycles. The photocatalytic reduction efficiency of Cr(VI) were calculated from the following expression:

$$\eta = (C_0 - C_t)/C_0 \times 100\% \text{----------(3)}$$

where $\eta$ is the photocatalytic degradation efficiency; $C_0$ and $C_t$ are the concentration of Cr(VI) before and after photocatalytic reaction [38].

# 4. Results and Discussion

## 4.1 Structural study

### 4.1.1 X-ray diffraction (XRD) analysis

Figure 7a shows XRD patterns of ZnAl LDH before and after calcination (ZnAl-MMO), and AgI, ZnAl-LDH, and cellulose templated-MMO-AgI. Before calcinations of the ZnAl-LDH samples, the diffraction peaks at 2θ = 11.8°, 23.5°, 34.6°, 39.2°, 46.8°, 60.1° and 61.6° were observed with (003), (006), (012), (015), (018), (110) and (113) planes, which is an indication of the distinctive well-crystalized hydrotalcite-like LDH materials formed (JCPDS card No. 048-1023)[32]. Upon calcination, the layer structure of ZnAl-LDH was destroyed and thus the diffraction peaks totally distributed. New and strong diffraction peaks were picked out in the XRD pattern of ZnAl-MMO composite. The intensity of diffraction peak increase with the

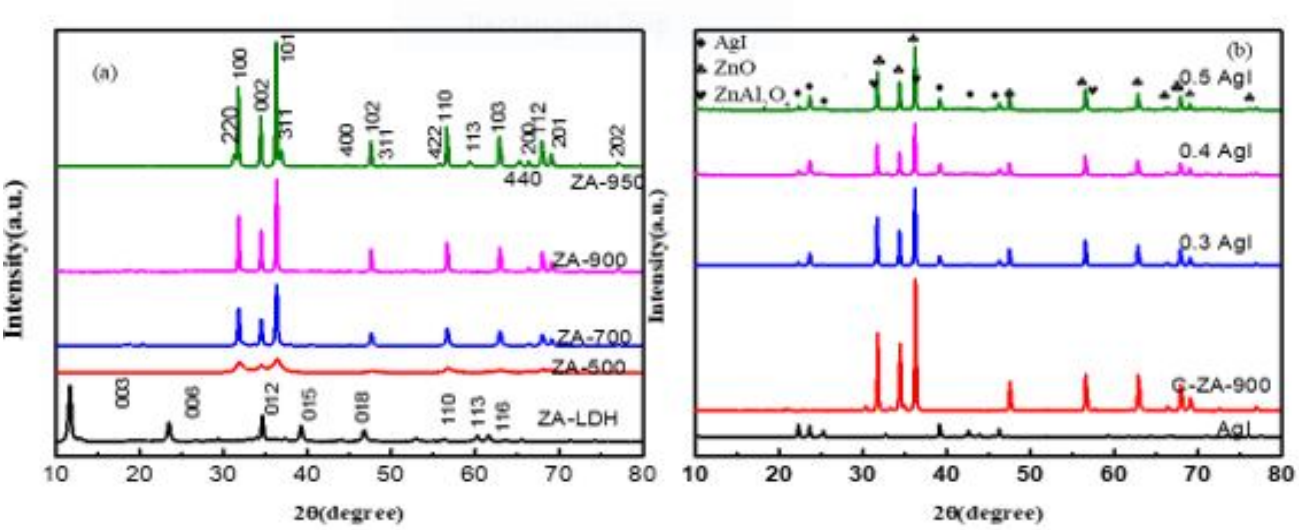


Figure 7. XRD diffraction peaks (a) ZA LDH and calcined at (500, 700, 900 and 950℃) (b) cellulose templated calcined ZA at various weight percent AgI.

calcination temperature. When the temperature was 500℃, the material is showed less crystalline. As temperature increased to 950℃, the deflection peak intensity increased and $ZnAl_2O_4$ phase visualized clearly. The diffraction peaks at 31.8° (100), 34.5° (002), 36.3° (010), 47.6° (102), 56.7° (110), 62.9° (103) and 68.0° (112) the standard data of the ZnO is matched well with hexagonal wurtzite phase (JCPDS No. 36- 1451) and the diffraction peaks at 31.4°, 36.9°, 44.8°, 49.1°, 55.6°,

65.2° is due to formation of cubic $ZnAl_2O_4$ at (220), (311), (400), (331), (422) and (440) planes (JCPDS No 005-0669)

Moreover, the AgI diffraction peaks at 2θ values of $22.08^0$, $23.7^0$, $25.33^0$, $39.2^0$, $42.64^0$ and $46.32^0$ which are indicated as the (100), (002), (101), (110), (103) and (112) planes of β-AgI (JCPDS 009-0374) and it can be observed on C-ZA-AgI [36]. In fact, hexagonal β-AgI and cubic α-AgI always overlap at ambient temperature. It can be proved that all peaks of α-AgI coexisted with the peaks of (002), (110), (112) of β–AgI. The peak of (003) centered at 2θ = 11.8 indicates the intercalation of $CO_3^{2-}$ anions and water molecules into the layer interspace [18]. From the XRD pattern of Zn/AL LDH and cellulose template Zn/Al LDH, there is small variations of 2θ angle. Cellulose templated. LDH peak shift to the right [170]. This indicates the templated cellulose during calcination left carbon residuals that intercalate or deposed on the surface of MMO particles. Fig 6b. shows various amount of AgI composition on calcined ZnAl LDH. The shift to the right results average crystalline particles increase. The diffraction peak of AgI increased at weight percent. 40. And decrease at 30 and 50. This may be composition ratio peak has high diffraction intensity relative to the others, it may be indicated well crystalline formation of the composite.

### 4.1.2. Morphologic structure analysis

AgI nanoparticles have been shown nearly spherical particles using Scanning Electron Microscopy (SEM) figure 8(a). These particles are formed sheet like structure due to aggregation of very small particles. It can be seen that the sample has no unique morphology and the agglomeration is high. Pure AgI precipitated in irregular morphology form which is probably created by the agglomeration of primary AgI particles. When the hydrated MCC comes in contact with the $Zn^2p$ and $Al^3p$ metal ions, there builds an electrostatic attraction which the adhering between MCC and the metal cations Figure 8(b). This can be clear in a way that electron-rich oxygen atoms of the polar hydroxyl groups of MCC are expected to interact with the electron-shortage transition metal cations. The effect of MCC on LDH synthesis has obtained significant variations on the morphology of the particles keeping the layered structure integral, the particles are seen to be depositing on the surface of MCC. The force of interaction of the hexagonal platelets with its edges has less proximity for a stable adhesion. Hence, there is a high chance of the attached particles to get isolated from the template which needs the particle to develop to a larger size independent of

the template. It is understood more from this image that the LDH has grown one upon the other over the MCC forming interconnected networks. This is clearly different from the regular shape and arrangement of LDH as shown in Figure 8(c). The ZnAl-LDH without cellulose displayed evident flat shaped particles with small aggregation, which was the indicative structure of a hydrotalcite-like compounds. The particles have incomplete hexagonal structures, and occur as small agglomerates consisted of several sandwiched platelets. The LDH in the absence of MCC shows the hexagonal characteristic. Figure 8(d) morphology confirms that the templating MCC is removed from the composite by calcination. After calcination at 900℃ the material possesses an MCC printed appearance of LDH with cylindrical hollow structures. Hence, we can observe that

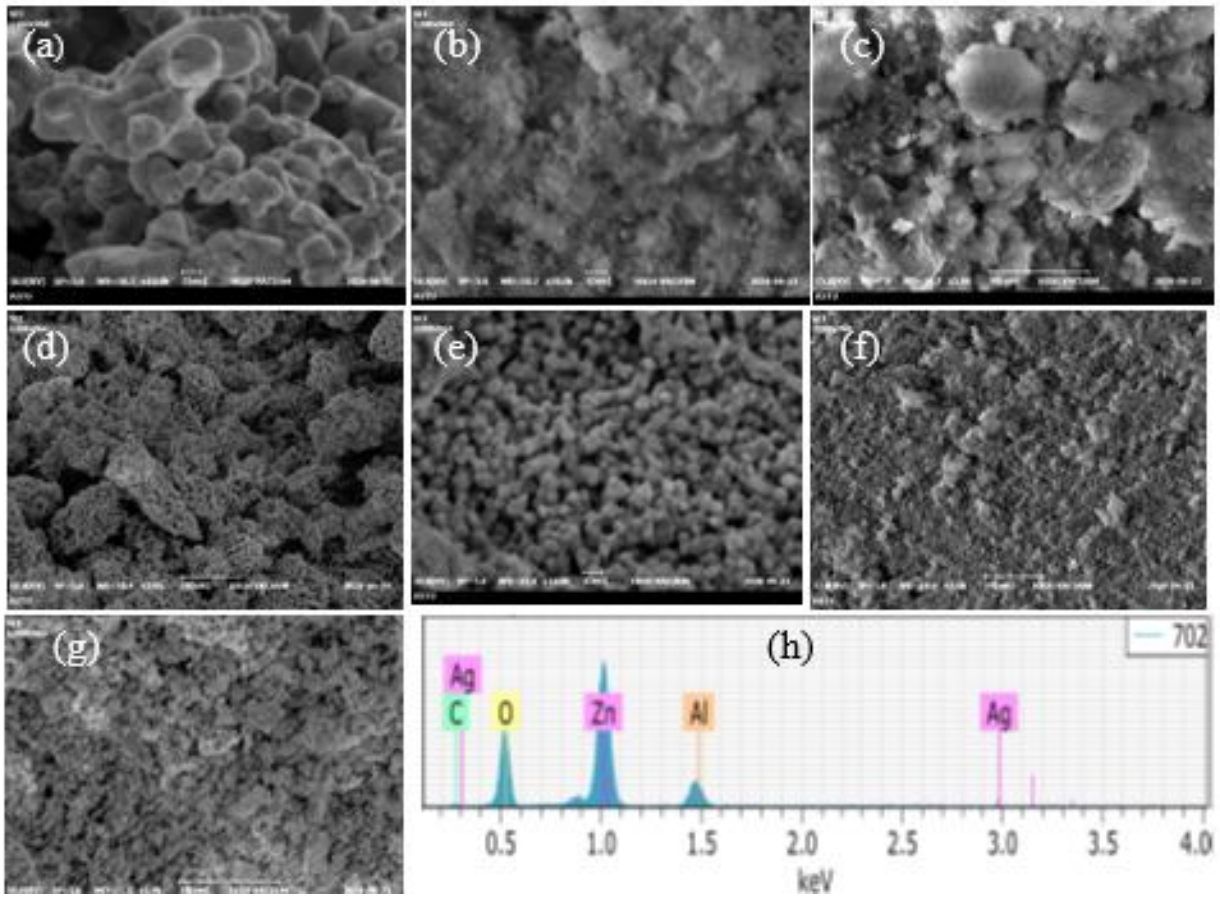


Figure 8. SEM (a) AgI, (b) C-LDH, (c) LDH, (d) C-ZA-MMO, (e) 40%AI-C-ZA-MMO, (f) ZA-MMO, (g) 40%AI-ZA-MMO and (h) EDXS ZA- MMO-AgI

the imaginable property of the template and its consequent removal, which has led may be to the formation of a porous chain in LDH as literatures analysis. In the case of LDH, the availability of

MCC in LDH synthesis was with the aim of providing a uniform distribution for the mass of inorganic LDH particles formed on MCC. In figure 8(e) the morphology of calcined cellulose templated LDH at 900℃ refluxed and combined with AgI was exhibited like uniform distribution, and small spherical shapes without insignificant agglomeration. The structure of calcined cellulose templated LDH combined with AgI changed radically. This change may have been occurred due to reflux of calcined LDH and uniform precipitation deposition of AgI on the surface of MMO catalyst. It is almost free from agglomeration. It indicates the aim of cellulose templating process achieved. Calcined ZnAl LDH at 900 ℃ produces some porous structure particles with destroy the hydrotalcite frame work Figure 8f. Calcination at elevated temperature leads the memory effect disappears. That shows more irregular flake morphology and agglomeration of many round edged small particles observed. In figure 8(g) the calcined LDH composed with AgI has uniform distribution and it seems have flake like structure unlike cellulose templated MMO composite. Agglomeration slightly high compared to figure 8(e). In order to identify the amount of various elements present in the composition of photocatalysts were confirmed by EDS result (figure 8(h)) and there are no other impurities in the composition. Except carbon residuals from cellulose during calcination.

### 4.1.3. UV–Vis spectra

The UV–Vis diffuse reflectance spectra (DRS) of 40%-AgI/ZA MMO, C-ZA MMO and ZA MMO samples are presented in figure 8. 40%-AgI-C-ZA MMO has high absorption in the visible region. Then 40%-AgI-ZA MMO has better adsorption in visible range relative to the others. After the modification of AgI, the photocatalyst exhibits distinct absorption in the visible light range (wavelength < 450 nm). Therefore, addition of AgI onto calcined ZA could enhanced the absorption wavelength start 450 nm which shows the photocatalyst degradation improvement source could induce a strong and increased absorption band in the visible region. Meanwhile, the bandgap energy (Eg) of the as-prepared AgI/C-ZA semiconductors composite can be calculated by the Kubelka-Munk equation. From the plots of $(\alpha hV)^2$ versus energy (hV) in Figure 9 b, the bandgap of 0.4Ag/c-ZA were calculated using the following formula.

$$(\alpha hV)^{1/n} = k\,(hV - E_g) \quad \text{----------(5)}$$

Where: the exponent n is 2 for direct-allowed transitions and 1/2 for indirect allowed transition; k is an energy-independent constant and $E_g$ is referred as the optical band gap.

Thus, $E_g$ of 0.4Ag/C-ZA, C-ZA and ZA are approximately equal to 2.6 eV, 2.93 and 2.98 respectively. This band gap result obtained due to composite heterojunction effect of MMO and AgI.

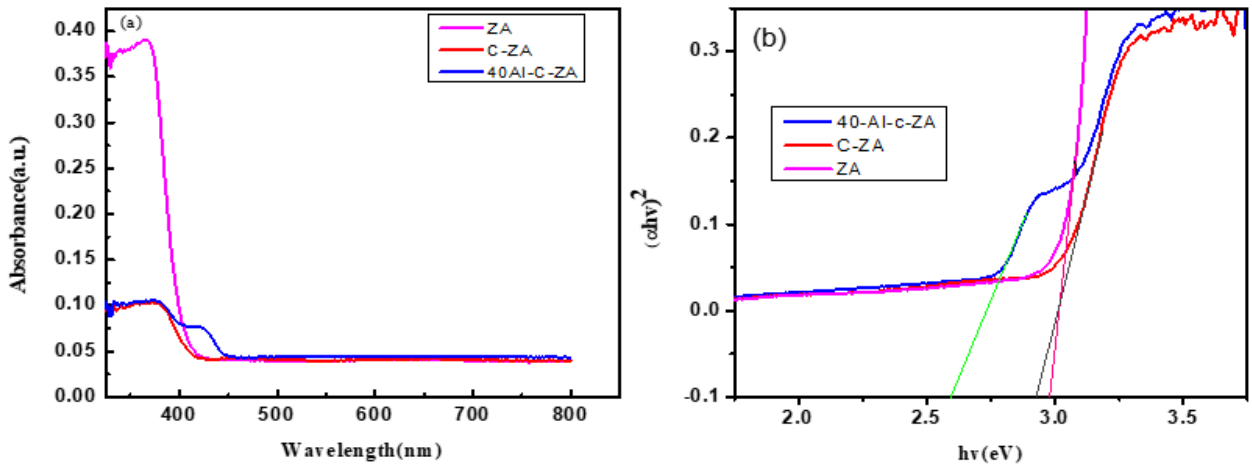


Figure .9. (a) UV–vis diffuse reflectance spectra of ZA-LDH, 40%AI-C-ZA and C-ZA-LDH and (b) Energy gap of ZA LDH, 40% AI-C-ZA and C-ZA LDH

## 4.2 Photocatalytic reduction Cr(VI) removal using C-ZA MMO-AgI composites

Figure 9a shows the photocatalytic removal of Cr(VI) using C-MMO-AgI composites, C-ZnAl MMO, and AgI under UV-Vis light. The removal efficiencies of triple C-MMO- ZnAl-AgI composites for Cr(VI) exceeded those of LDH and AgI. The reduction rates of triple C-MMO-AgI composites were selected by their AgI contents. Comparatively, LDH presented shorter reaction equilibrium time than AgI and C-MMO-AgI-30%, C-MMO-AgI-40%, C-MMO-AgI-50%, because the LDH high adsorption property. However, the removal rates of C-MMO-AgI-30%, C-MMO-AgI-40% and C-MMO-AgI-50% were superior compared to that of LDH. It resulted from the formation of heterojunction between AgI and C-MMO, which would usually be important for enhancing the separation of the electron–hole pairs over catalysts. The presence of such types photocatalytic reduction occur on aqueous Cr(VI) using C-ZnAl-MMO/AgI as the photocatalyst under UV-Vis light irradiation. The aqueous Cr(VI) solution was almost stable under Visible light

(blank experiment). When initial Cr(VI) concentrations of 20 mg/L $K_2Cr_2O_7$ with 40AI-C-ZA-MMO photocatalytic removal percentage of aqueous Cr(VI) was tend to be 87% in 90 min and 40% AI-MMO photocatalytic percentage removal of aqueous Cr(VI) was 66.7%. The difference in photocatalytic performance between 40 AI-C-MMO. and 40 AI-MMO was due to cellulose template LDH precursor may be while increase due to porosity and specific surface area of 40 AI-C-ZA-MMO.

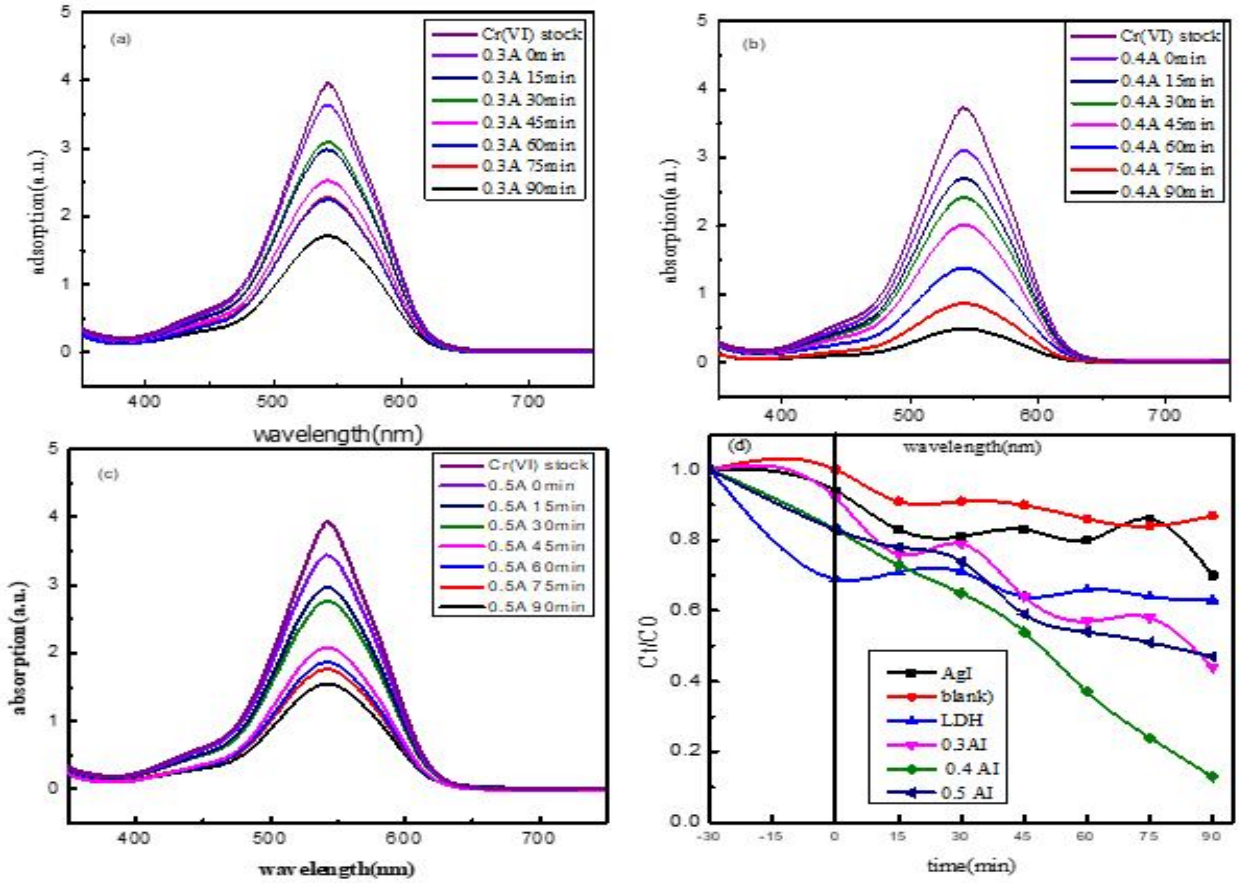


Figure 10. Time-dependent degradation spectral of DPC–Cr(VI) complex solutions (a) using 30% of AgI, (b) using 40% of AgI, (c) using 50% of AgI and (d) The $C_t/C_0$ photoreduction profile a function of time

### 4.2.1. Kinetics of photocatalytic reduction

The photocatalytic reduction kinetics of Cr(VI) under UV-visible light irradiation was assessed and the results showed that the changes of Cr(VI) concentration versus reaction time over 40AgI-ZnAl-MMO composite photocatalysts good matched with pseudo-first-order kinetics plot by the

equation of ln ($C_t/C_0$)=−kt, where t, $C_0$, and $C_t$ are the reaction time, Cr(VI) concentration (mg.$L^{-1}$) at adsorption/desorption equilibrium without light irradiation, Cr(VI) concentration (mg·$L^{-1}$) at time t(min); k indicates the apparent pseudo-first-order rate constant ($k_{app}$/min−1). The values of rate constant ($k_{app}$/$min^{-1}$) are obtained from the slope of the plot of ln($C_t/C_o$) versus time t. The linear fitting curve of ln($C_t/C_o$) versus time during 0–90 min with different catalysts and blank Cr(VI) was plotted and presented in Figure 10. This figure indicates that photocatalytic degradation of 40 AgI/C-ZAMMO over all photocatalysts has good degradation rate. LDH has better degradation rate constant during adsorption desorption time but almost became constant after illumination of light.

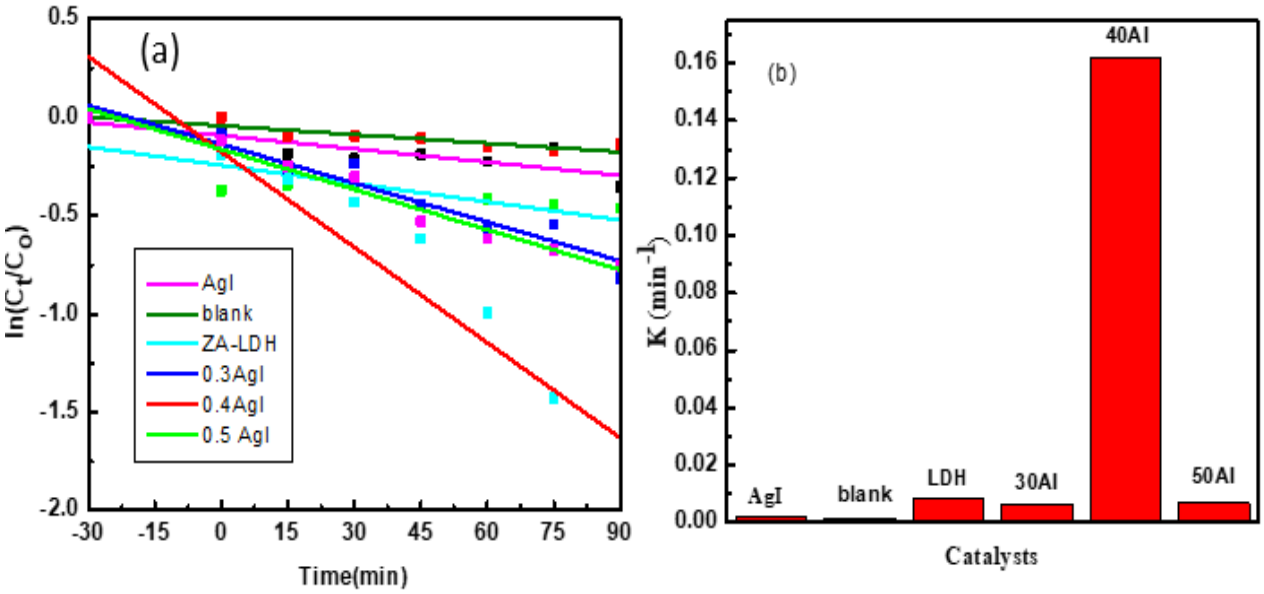


| Catalysts | AgI | Blank | LDH | 0.3 AI | 0.4 AI | 0.5 AI |
|---|---|---|---|---|---|---|
| K | 0.00225 | 0.00148 | 0.0081 | 0.0066 | 0.16173 | 0.00682 |
| $R^2$ | 0.65612 | 0.8065 | 0.62832 | 0.92273 | 0.8587 | 0.96886 |

Figure 11. (a) Plot of ln($C_t/C_0$) versus time for reduction of Cr(VI), (c) The kinetic rate constants for AgI, LDH, 0.3AI, 0.4AI and 0.5AI catalysts.

#### 4.2.2. Effect of calcination temperature on the MMO photocatalytic degradation

To fully maintain the photocatalytic performance of the calcined MMO composites, the memory effect of MMO must be blocked. With increase the calcination temperature the photocatalytic activity clearly raises owing to the starting of formation of ZnO to around 350℃. The samples show the photocatalyst activity highest at 900℃ and below and above this calcination temperature the photocatalyst activities were decreased. This can be represented based on crystallization[171] and adsorption also has important factor for photocatalyst reduction process. As shown in the Figure 11. the adsorption desorption equilibrium in dark region was best on 900℃ calcination

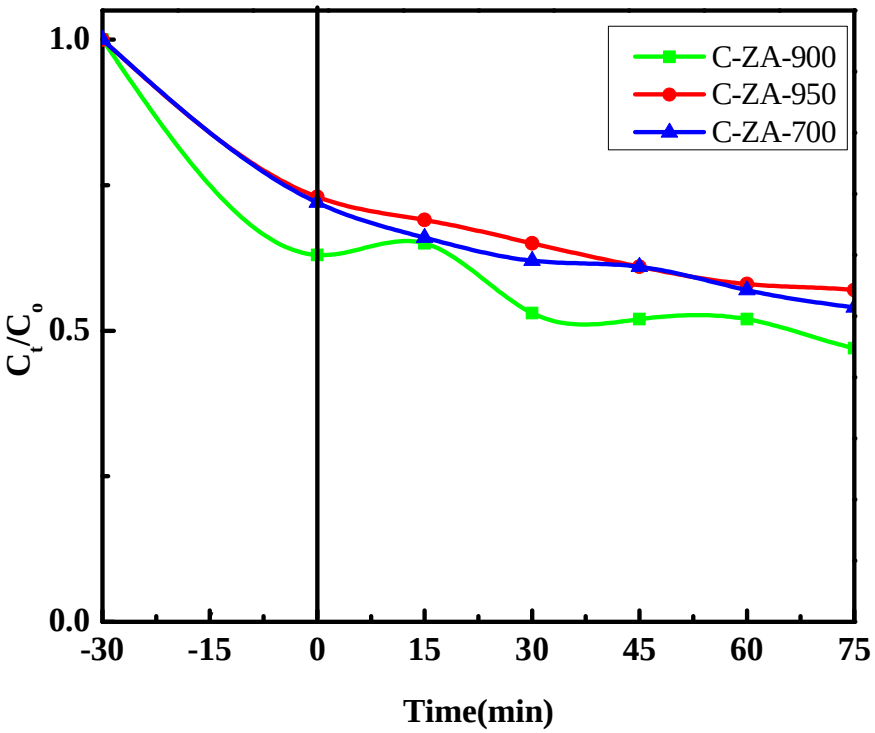


Figure 12. Effect of calcination temperature with 47.5 Weight % of AgI

temperature. At 700℃ both adsorption and photocatalyst reduction shows low performance than that of 900$^{℃}$. It may be occurred due to photocatalyst reduction of ZnO increase with calcination temperature. Beyond 900℃ the photocatalyst reduction decrease with further increasing calcination temperature to 950℃. This result can be assigned a partition of ZnO in the calcined photocatalyst would be transformed into $ZnAl_2O_4$, which is not important in the process of

photocatalyst reduction. However, pure ZnO exhibited moderate photocatalyst performance, while LDH based precursor of ZnO enhance highly photocatalyst activity [171].

### 4.2.3. Effect of initial pH of the solution on the photocatalytic reaction

The solution's pH is one of the most important parameters in photocatalytic process. The effect of initial pH on the reduction of Cr(VI) using 40%AI-C-ZnAl-MMO photocatalyst was investigated by varying the initial pH from 3.5 to 11 at an initial $K_2Cr_2O_4$ concentration of 20 mg/L. The photoreduction efficiency of Cr(VI) was increased from 87% to 91% within 90 min visible light irradiation with decreasing the initial pH values from 7.48 (the pH of the original solution) to 3.5, whereas only 24% of Cr(VI) was photocatalytically removed at pH 11 within 90 min. The phenomenon shows that higher photoreduction efficiency towards Cr(VI) was obtained in acidic solutions than in alkaline solutions was in accordance with the reported results. In acidic-solution, the surface of the photocatalyst may be highly protonated and thus leads to strong electrostatic attraction towards the main species $HCrO_4^-$ or $Cr_2O_7^{2-}$ of chromium anions in low pH solution. And Cr(VI) is highly stable in basic solution. Because in acidic solution hole scavengers available unless recombination of exited electron with hole occurred [7].The highest photocatalytic activity was obtained at pH 1- 3. It is probably due to the oxidative ability of photo-generated holes and reductive ability of conduction band electrons which are greatly influenced by PH. The valence band edge shifted to more negative potential at higher pH, and the oxidative ability decreased subsequently, which leads to inhibited degradation of Cr(VI) changed from $HCrO_4^-$ to $CrO_4^{2-}$ at pH>6. Since $CrO_4^{2-}$ [$E0(CrO4^{2-}/Cr(OH)_3$) = -0.13 V vs [NHE] is a much weaker oxidant than $HCrO_4^-$ [$E0(HCrO_4^-/Cr^{3+}$) = 1.35 V vs NHE] [38], the thermodynamic driving fore between conduction band and Cr(VI)/Cr(III) becomes narrower at high pH which was unfavorable for the reduction of Cr(VI). Anyway, high reduction rate of Cr(VI) can still be observed at near neutral pH, which will be beneficial for future wastewater treatment with wide pH range [36].

## 4.3. Effect of AgI-Zn/Al molar ratio on the photocatalytic reaction

The optimum value of AgI weight ratio catalyst was identified by using UV-visible irradiation exposing of Cr(VI) aqueous solution with 10, 20, 30, 40 and 50% AgI deposited on ZA MMO composite. The best performance was obtained at 40% AgI deposition. This may be occurred below 40% AgI precipitation deposition the amount of electron excitation with ratio decreased

relative to the parent composite and above 40% the agglomeration of AgI weight percent increased and the functional surface of $ZnO/ZnAl_2O_4$ may covered with AgI photocatalyst. That has high recombination rate.

### 4.4. The mechanism of enhanced photocatalytic activity for Cr(VI) reduction of $AgI/ZnOZnAl_2O_4$

On the basis of the experimental results presented in this work, a synergistic mechanism between ZnO, AgI and $ZnAl_2O_4$ triple phases in the composite for photocatalytic reduction improvement of Cr(VI) is proposed. Herein, electron-hole pairs can easily be produced on $AgI/ZnO/ZnAl_2O_4$ due to the existence of visible-light-active substance of AgI. When the photocatalyst irradiated with visible light the photo energy higher than the band gap of AgI, the e- in the valance band (VB) exited in to the conduction band (CB), results the same amount of holes. The pure AgI the photogenerated e–h readily recombines. However, due to the presence of ZnO and the potential of the conduction band of AgI more negative than ZnO. Then electrons transferred across the heterojunctions structure to the conduction band of ZnO.This leads to the enhanced life time by suppressing the recombination of $h^+$ and $e^-$. Such process is energetically desirable and then efficiently suppress electron-hole recombination, leading to large numbers of electrons on the ZnO surface. Because the CB position of ZnO is more negative than the reduction potential of E $(Cr_2O_7^{2-}/Cr^{3+})$ =+1.33 V (vs. NHE), the accumulated photoinduced electron as the same time reduce $Cr^{6+}$ to $Cr^{3+}$ (Eq. (4.)). Meanwhile, due to the more positive VB position of AgI than the oxidation potential of $E^0(H_2O/O_2)$ =1.23 V (vs. NHE), the holes oxidize water to form $O_2$ (Eq. (5)). The efficient separation of electron-hole pairs is the key factor for the high photocatalytic activity of ZnAl-MMO nanocomposite towards Cr(VI) reduction.

$Cr_2O_7^{2-} + 14H^+ + 6e \rightarrow 2Cr^{3+} + 7H_2O^-$ ---------- (4)

$2H_2O + 4H^+ \rightarrow O_2 + 4H^+$---------- (5)

Additionally, because the CB position of AgI (-0.42) is more negative than the reduction potential of $E_o(O_2/O_2^{\bullet-})$ = −0.33 eV (vs. NHE), apart of electrons at the CB of AgI could react with $O_2$ adsorbed on the surface of the composite to yield $O_2^{\bullet-}$, which is capable to reduce $Cr^{6+}$ to $Cr^{3+}$ As the electron transfer from CB of AgI to that of ZnO is energetically favorable. $ZnAl_2O_4$ is used mainly as a support of photocatalyst composite [32]

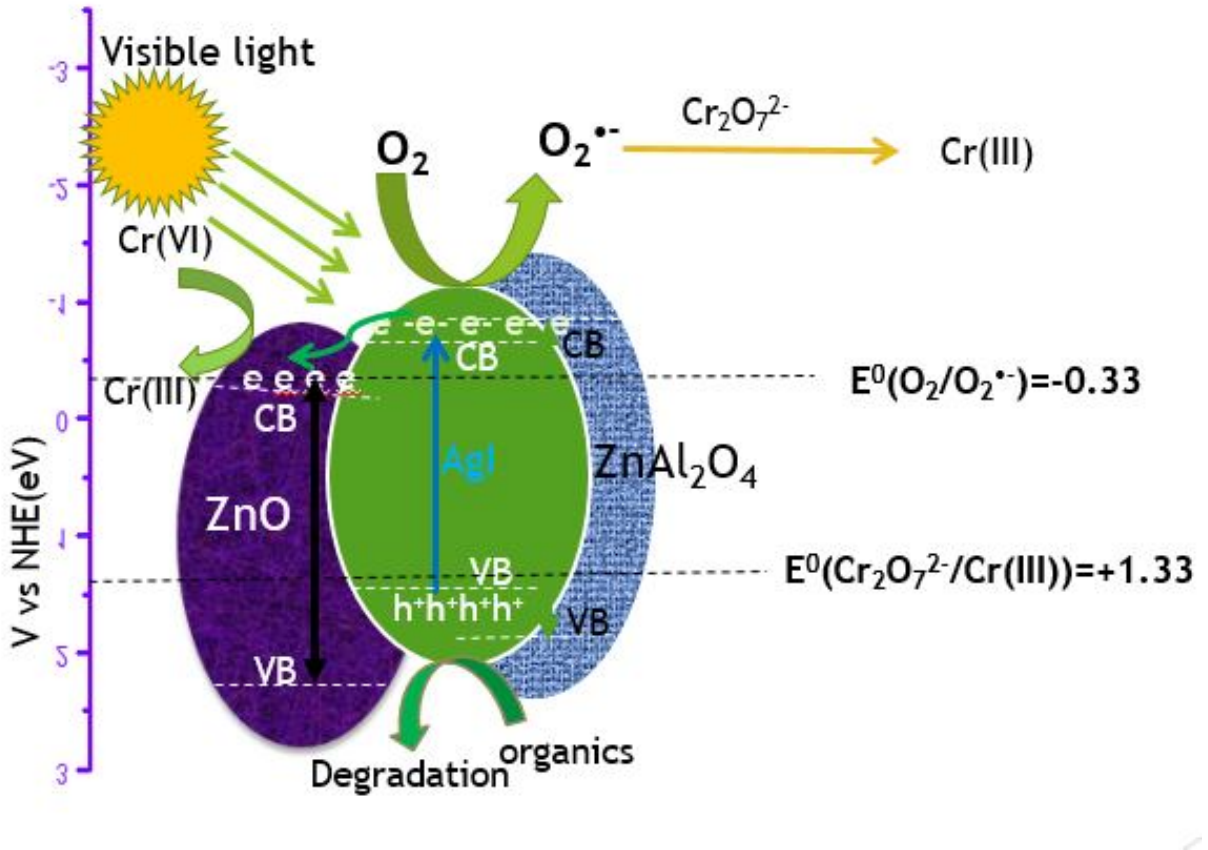


Figure 13. Schematic illustration of the mechanism of electron-hole separation and transport and Photocatalytic activity of ZnAl-MMO photocatalyst under visible light irradiation

### 4.5. Reusability and stability of the photocatalyst

The reusability of c-ZnAl-AgI test was performed for 4 cycle of photocatalyst application. As shown in the bar graph, the performance decreases within a cycle of Cr(VI) reduction. This may be during washing and drying in each cycle, AgI washed away with distilled water. Due the low adhering formation of precipitating deposition on the surface of ZnAl MMO, dissolution and photocorrosion.

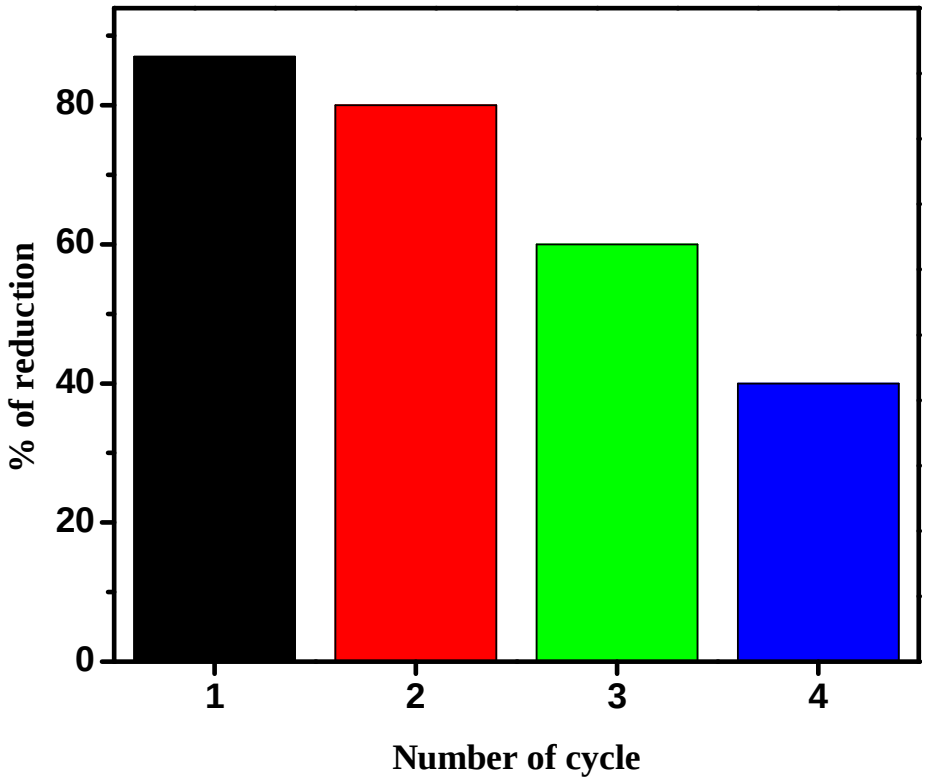


Figure 14. Reusability chart

# 5. Conclusion and Recommendation

## 5.1 Conclusion

In present work cellulose templated ZnAl layered double hydroxide prepared via simple co-precipitation process, and ZnAl mixed metal oxides/AgI photocatalyst composite prepared by AgI deposited on the surface of ZnAl MMO powder after refluxing with ultra-sonicate and simple precipitation deposition process. Significantly advanced photocatalyst C-ZnAl MMO/AgI achieved for the application of visible light irradiation of Cr(VI) reduction. The prepared photocatalyst were characterized using XRD, SEM, EDS and DRS. AgI semiconductor was applied to enhance the C-ZnAl MMO photocatalyst from UV irradiation functionality to visible light. From the optimization of AgI to ZnAl-MMO, weight percent of deposition 40% performed best efficiency (87% reduction). This occurred due to uniform distribution of the effective cite of AgI on the surface of $ZnOZnAl_2O_4$. 50% of AgI had low performance which might be the agglomeration of AgI and cover the effective surface of C-ZnAl MMO (53% reduction). 30% of AgI also shows low efficiency, that may be occurred due to less effective site of AgI caused decrease participation of the photogenerated excited electrons transfer to conduction band of ZnO (56%). It was observed the performance of cellulose-templated and without cellulose have different photocatalytic efficiency, with Cellulose-templated ZnAl-MMO with AgI resulted 86% but without cellulose 66% Cr(VI) reduction observed.

## 5.2. Recommendation

Cellulose used for the templated synthesis of ZnAl LDH was not optimized. Then by optimization of cellulose used as a templated synthesis of ZnAl LDH may be enhance the performance of photocatalyst. The other one in Cr (VI) reduction using organic pollutant materials serves as hole scavengers advised in different literatures. But in this work it was not performed. So organic pollutant addition in Cr(VI) aques solution may increase the efficiency of photocatalyst reduction performance. By using photocatalyst served as for degradation of organic pollutants and inorganic Cr(VI) reduction simultaneously.

# 6. **Reference**


1. Kumar, V., et al., Global evaluation of heavy metal content in surface water bodies: A meta-analysis using heavy metal pollution indices and multivariate statistical analyses. Chemosphere, 2019. **236**: p. 124364.
2. Zheng, Y., et al., 3D hierarchical graphene oxide-NiFe LDH composite with enhanced adsorption affinity to Congo red, methyl orange and Cr(VI) ions. J Hazard Mater, 2019. **369**: p. 214-225.
3. Lei, C., et al., Superb adsorption capacity of hierarchical calcined Ni/Mg/Al layered double hydroxides for Congo red and Cr(VI) ions. J Hazard Mater, 2017. **321**: p. 801-811.
4. Giri, S., et al., Development of a new noncarcinogenic heavy metal pollution index for quality ranking of vegetable, rice, and milk. Ecological Indicators, 2020. **113**: p. 106214.
5. Abdullah, N., et al., Recent trends of heavy metal removal from water/wastewater by membrane technologies. Journal of Industrial and Engineering Chemistry, 2019. **76**: p. 17-38.
6. Onchoke, K.K. and S.A. Sasu, Determination of Hexavalent Chromium (Cr(VI)) Concentrations via Ion Chromatography and UV-Vis Spectrophotometry in Samples Collected from Nacogdoches Wastewater Treatment Plant, East Texas (USA). Advances in Environmental Chemistry, 2016. **2016**: p. 1-10.
7. Singanan, M. and E. Peters, Removal of toxic heavy metals from synthetic wastewater using a novel biocarbon technology. Journal of Environmental Chemical Engineering, 2013. **1**(4): p. 884-890.
8. Bankole, M.T., et al., Selected Heavy Metals Removal From Electroplating Wastewater by Purified and Polyhydroxylbutyrate Functionalized Carbon Nanotubes Adsorbents. Sci Rep, 2019. **9**(1): p. 4475.
9. Agrawal, S.G., R.L. Fimmen, and Y.-P. Chin, Reduction of Cr(VI) to Cr(III) by Fe(II) in the presence of fulvic acids and in lacustrine pore water. Chemical Geology, 2009. **262**(3-4): p. 328-335.
10. Zhang, B., et al., Rapid and effective removal of Cr(VI) from aqueous solution using exfoliated LDH nanosheets. Colloids and Surfaces A: Physicochemical and Engineering Aspects, 2017. **520**: p. 399-408.
11. Cronje, K.J., et al., Optimization of chromium(VI) sorption potential using developed activated carbon from sugarcane bagasse with chemical activation by zinc chloride. Desalination, 2011. **275**(1-3): p. 276-284.
12. Zare, E.N., A. Motahari, and M. Sillanpaa, Nanoadsorbents based on conducting polymer nanocomposites with main focus on polyaniline and its derivatives for removal of heavy metal ions/dyes: A review. Environ Res, 2018. **162**: p. 173-195.
13. Arantes de Carvalho, G.G., et al., Hybrid polysaccharide beads for enhancing adsorption of Cr(VI) ions. Colloids and Surfaces A: Physicochemical and Engineering Aspects, 2018. **558**: p. 144-153.
14. Lin, Y.-C. and S.-L. Wang, Chromium(VI) reactions of polysaccharide biopolymers. Chemical Engineering Journal, 2012. **181-182**: p. 479-485.
15. Wu, X.-W., H.-W. Ma, and Y.-R. Zhang, Adsorption of chromium(VI) from aqueous solution by a mesoporous aluminosilicate synthesized from microcline. Applied Clay Science, 2010. **48**(3): p. 538-541.

16. Yuan, Q., et al., $Cu_2O/BiVO_4$ heterostructures: synthesis and application in simultaneous photocatalytic oxidation of organic dyes and reduction of Cr(VI) under visible light. Chemical Engineering Journal, 2014. **255**: p. 394-402.
17. Ullah, I., et al., Biosorption of chromium onto native and immobilized sugarcane bagasse waste biomass. Ecological Engineering, 2013. **60**: p. 99-107.
18. Hu, B., et al., Pseudo-Janus Zn/Al-based nanocomposites for Cr(VI) sorption/remediation and evolved photocatalytic functionality. Chemical Engineering Journal, 2015. **277**: p. 150-158.
19. Gusain, R., et al., Adsorptive removal and photocatalytic degradation of organic pollutants using metal oxides and their composites: A comprehensive review. Adv Colloid Interface Sci, 2019. **272**: p. 102009.
20. Prasad, C., et al., An overview of semiconductors/layered double hydroxides composites: Properties, synthesis, photocatalytic and photoelectrochemical applications. Journal of Molecular Liquids, 2019. **289**: p. 111114.
21. Lin, S.-T., et al., Layered double hydroxides intercalated with sulfur-containing organic solutes for efficient removal of cationic and oxyanionic metal ions. Applied Clay Science, 2018. **162**: p. 443-453.
22. de Almeida, M.F., et al., Enhanced photocatalytic activity of $TiO_2$-impregnated with MgZnAl mixed oxides obtained from layered double hydroxides for phenol degradation. Applied Surface Science, 2015. **357**: p. 1765-1775.
23. Berner, S., et al., Cu/Al and Cu/Cr based layered double hydroxide nanoparticles as adsorption materials for water treatment. Journal of Industrial and Engineering Chemistry, 2018. **59**: p. 134-140.
24. Jia, X., et al., Fabrication and Bifunctional Electrocatalytic Performance of Ternary CoNiMn Layered Double Hydroxides/Polypyrrole/Reduced Graphene Oxide Composite for Oxygen Reduction and Evolution Reactions. Electrochimica Acta, 2017. **245**: p. 59-68.
25. Guo, Q., et al., Core-shell structured ZnO@Cu-Zn–Al layered double hydroxides with enhanced photocatalytic efficiency for $CO_2$ reduction. Catalysis Communications, 2016. **77**: p. 118-122.
26. Yang, Z.-z., et al., A review on strategies to LDH-based materials to improve adsorption capacity and photoreduction efficiency for $CO_2$. Coordination Chemistry Reviews, 2019. **386**: p. 154-182.
27. Yang, Y., et al., Synergistic adsorption and photocatalytic reduction of Cr(VI) using Zn-Al-layered double hydroxide and $TiO_2$ composites. Applied Surface Science, 2019. **492**: p. 487-496.
28. Gao, C., et al., Removal of hexavalent chromium ions by core-shell sand/Mg-layer double hydroxides (LDHs) in constructed rapid infiltration system. Ecotoxicol Environ Saf, 2018. **166**: p. 285-293.
29. Hadnadjev-Kostic, M., et al., Photo-induced properties of photocatalysts: A study on the modified structural, optical and textural properties of $TiO_2$ –ZnAl layered double hydroxide based materials. Journal of Cleaner Production, 2017. **164**: p. 1-18.
30. Hasija, V., et al., Carbon quantum dots supported AgI /ZnO/phosphorus doped graphitic carbon nitride as Z-scheme photocatalyst for efficient photodegradation of 2, 4-dinitrophenol. Journal of Environmental $_{\text{Chemical}}$ Engineering, 2019. **7**(4): p. 103272.
31. Szostak, K. and M. Banach, Sorption and photocatalytic degradation of methylene blue on bentonite-ZnO-CuO nanocomposite. Journal of Molecular Liquids, 2019. **286**: p. 110859.

32. Yuan, X., et al., Photocatalytic Cr(VI) reduction by mixed metal oxide derived from ZnAl layered double hydroxide. Applied Clay Science, 2017. **143**: p. 168-174.
33. Wang, Q., et al., Fabrication of beta-phase AgI and $Bi_2O_3$ co-decorated $Bi_2O_2CO_3$ heterojunctions with enhanced photocatalytic performance. J Colloid Interface Sci, 2019. **547**: p. 1-13.
34. Zhang, C., et al., Hydrated-Metal-Halide-Based Deep-Eutectic-Solvent-Mediated NiFe Layered Double Hydroxide: An Excellent Electrocatalyst for Urea Electrolysis and Water Splitting. Chemistry – An Asian Journal, 2019. **14**(17): p. 2995-3002.
35. Di, G., et al., Targeted modulation of g-$C_3N_4$ photocatalytic performance for pharmaceutical pollutants in water using ZnFe-LDH derived mixed metal oxides: Structure-activity and mechanism. Sci Total Environ, 2019. **650**(Pt 1): p. 1112-1121.
36. Wang, Q., et al., Preparation of AgI sensitized amorphous TiO(2) as novel high-performance photocatalyst for environmental applications. J Colloid Interface Sci, 2015. **448**: p. 407-16.
37. Roy, S., J.-W. Rhim, and L. Jaiswal, Bioactive agar-based functional composite film incorporated with copper sulfide nanoparticles. Food Hydrocolloids, 2019. **93**: p. 156-166.
38. Zhao, W., et al., Simultaneous removal of tetracycline and Cr(VI) by a novel three-dimensional AgI/$BiVO_4$ p-n junction photocatalyst and insight into the photocatalytic mechanism. Chemical Engineering Journal, 2019. **369**: p. 716-725.
39. Wang, Q., et al., Facile synthesis of AgI/BiOI-$Bi_2O_3$ multi-heterojunctions with high visible light activity for Cr(VI) reduction. J Hazard Mater, 2016. **317**: p. 8-16.
40. Wang, Q., et al., Highly enhanced photocatalytic reduction of Cr(VI) on AgI/$TiO_2$ under visible light irradiation: Influence of calcination temperature. J Hazard Mater, 2016. **307**: p. 213-20.
41. Velmurugan, S., et al., Synthesis of novel and environmental sustainable AgI-$Ag_2S$ nanospheres impregnated g-$C_3N_4$ photocatalyst for efficient degradation of aqueous pollutants. Applied Surface Science, 2020. **500**: p. 143991.
42. Duan, Y., et al., Assembly of graphene on $Ag_3PO_4$/AgI for effective degradation of carbamazepine under Visible-light irradiation: Mechanism and degradation pathways. Chemical Engineering Journal, 2019. **359**: p. 1379-1390.
43. Mureseanu, M., et al., Green synthesis of g-$C_3$ $N_4$ /CuONP/LDH composites and derived g-$C_3$ $N_4$ /MMO and their photocatalytic performance for phenol reduction from aqueous solutions. Applied Clay Science, 2017. **141**: p. 1-12.
44. Hu, H., et al., Hierarchical porous Ni/Co-LDH hollow dodecahedron with excellent adsorption property for Congo red and Cr(VI) ions. Applied Surface Science, 2019. **478**: p. 981-990.
45. Mandal, S. and S. Mayadevi, Cellulose supported layered double hydroxides for the adsorption of fluoride from aqueous solution. Chemosphere, 2008. **72**(6): p. 995-8.
46. Zhang, G., et al., Layered double hydroxides-based photocatalysts and visible-light driven photodegradation of organic pollutants: A review. Chemical Engineering Journal, 2020. **392**: p. 123684.
47. Mohamed, F., M.R. Abukhadra, and M. Shaban, Removal of safranin dye from water using polypyrrole nanofiber/Zn-Fe layered double hydroxide nanocomposite (Ppy NF/Zn-Fe LDH) of enhanced adsorption and photocatalytic properties. Sci Total Environ, 2018. **640-641**: p. 352-363.
48. El-Sayed, M.E.A., Nanoadsorbents for water and wastewater remediation. Science of The Total Environment, 2020: p. 139903.

49. Chubar, N., et al., Layered double hydroxides as the next generation inorganic anion exchangers: Synthetic methods versus applicability. Adv Colloid Interface Sci, 2017. **245**: p. 62-80.
50. Akansha, J., et al., Treatment of dairy industry wastewater by combined aerated electrocoagulation and phytoremediation process. Chemosphere, 2020. **253**: p. 126652.
51. Vetrimurugan, E., et al., Human exposure risk to heavy metals through groundwater used for drinking in an intensively irrigated river delta. Applied Water Science, 2016. **7**(6): p. 3267-3280.
52. Wen, X.-J., et al., Recent developments on AgI based heterojunction photocatalytic systems in photocatalytic application. Chemical Engineering Journal, 2020. **383**: p. 123083.
53. Li, C., et al., Enhanced visible-light-induced photocatalytic performance of $Bi_2O_3$/ZnAl-LDH–C for dyes removal in water. Materials Letters, 2019. **244**: p. 215-218.
54. Ayangbenro, A.S. and O.O. Babalola, A New Strategy for Heavy Metal Polluted Environments: A Review of Microbial Biosorbents. Int J Environ Res Public Health, 2017. **14**(1).
55. Samer, M., Biological and Chemical Wastewater Treatment Processes. 2015.
56. Zwain, H.M., M. Vakili, and I. Dahlan, Waste Material Adsorbents for Zinc Removal from Wastewater: A Comprehensive Review. International Journal of Chemical Engineering, 2014. **2014**: p. 1-13.
57. Ahmaruzzaman, M. and V.K. Gupta, Rice Husk and Its Ash as Low-Cost Adsorbents in Water and Wastewater Treatment. Industrial & Engineering Chemistry Research, 2011. **50**(24): p. 13589-13613.
58. Zhelev, Z.M., et al., In situ assessment of health status and heavy metal bioaccumulation of adult Pelophylax ridibundus (Anura: Ranidae) individuals inhabiting polluted area in southern Bulgaria. Ecological Indicators, 2020. **115**: p. 106413.
59. Liu, W.R., et al., Comparisons of pollution characteristics, emission situations, and mass loads for heavy metals in the manures of different livestock and poultry in China. Sci Total Environ, 2020. **734**: p. 139023.
60. Tchounwou, P.B., et al., Heavy metal toxicity and the environment. Exp Suppl, 2012. **101**: p. 133-64.
61. Nagajyoti, P.C., K.D. Lee, and T.V.M. Sreekanth, Heavy metals, occurrence and toxicity for plants: a review. Environmental Chemistry Letters, 2010. **8**(3): p. 199-216.
62. Masindi, V. and K.L. Muedi, Environmental Contamination by Heavy Metals. 2018.
63. Lu, Y., et al., High performance NiFe layered double hydroxide for methyl orange dye and Cr(VI) adsorption. Chemosphere, 2016. **152**: p. 415-22.
64. Peng, G., et al., Removal of heavy metals from sewage sludge with a combination of bioleaching and electrokinetic remediation technology. Desalination, 2011. **271**(1-3): p. 100-104.
65. Bazrafshan, E., et al., Heavy metals removal from aqueous environments by electrocoagulation process- a systematic review. J Environ Health Sci Eng, 2015. **13**: p. 74.
66. Aljahdali, M.O. and A.B. Alhassan, Ecological risk assessment of heavy metal contamination in mangrove habitats, using biochemical markers and pollution indices: A case study of Avicennia marina L. in the Rabigh lagoon, Red Sea. Saudi J Biol Sci, 2020. **27**(4): p. 1174-1184.

67. Feng, Y., et al., Geo-accumulation vector model for evaluating the heavy metal pollution in the sediments of Western Dongting Lake. Journal of Hydrology, 2019. **573**: p. 40-48.
68. Zhou, Q., et al., Total concentrations and sources of heavy metal pollution in global river and lake water bodies from 1972 to 2017. Global Ecology and Conservation, 2020. **22**: p. e00925.
69. Alam, M., et al., The effects of organic amendments on heavy metals bioavailability in mine impacted soil and associated human health risk. Scientia Horticulturae, 2020. **262**: p. 109067.
70. Sang, C., et al., Effects of water impoundment and water-level manipulation on the bioaccumulation pattern, trophic transfer and health risk of heavy metals in the food web of Three Gorges Reservoir (China). Chemosphere, 2019. **232**: p. 403-414.
71. Huang, D., et al., Megamerger of biosorbents and catalytic technologies for the removal of heavy metals from wastewater: Preparation, final disposal, mechanism and influencing factors. J Environ Manage, 2020. **261**: p. 109879.
72. Wang, S., et al., Spatial distribution and assessment of the human health risks of heavy metals in a retired petrochemical industrial area, South China. Environmental Research, 2020: p. 109661.
73. Matheus, M.C., et al., Assessing the impact of hydraulic conditions and absence of pretreatment on the treatability of pesticide formulation plant wastewater in a moving bed biofilm reactor. Journal of Water Process Engineering, 2020. **36**: p. 101243.
74. Ahmed Basha, C., et al., Heavy metal removal from copper smelting effluent using electrochemical cylindrical flow reactor. J Hazard Mater, 2008. **152**(1): p. 71-8.
75. Ouyang, J., et al., Analysis of influencing factors of heavy metals pollution in farmland-rice system around a uranium tailings dam. Process Safety and Environmental Protection, 2020. **139**: p. 124-132.
76. Das, J., et al., Calcined Mg-Fe-CO(3) LDH as an adsorbent for the removal of selenite. J Colloid Interface Sci, 2007. **316**(2): p. 216-23.
77. Hudcova, B., et al., Stability and stabilizing efficiency of Mg-Fe layered double hydroxides and mixed oxides in aqueous solutions and soils with elevated As(V), Pb(II) and Zn(II) contents. Sci Total Environ, 2019. **648**: p. 1511-1519.
78. Grigoriev, S.A., et al., Current status, research trends, and challenges in water electrolysis science and technology. International Journal of Hydrogen Energy, 2020.
79. He, F., et al., Selective reduction of $Cu^{2+}$ with simultaneous degradation of tetracycline by the dual channels ion imprinted POPD-$CoFe_2O_4$ heterojunction photocatalyst. Chemical Engineering Journal, 2019. **360**: p. 750-761.
80. Safari, E., et al., Copper adsorptive removal from aqueous solution by orange peel residue carbon nanoparticles synthesized by combustion method using response surface methodology. Journal of Environmental Chemical Engineering, 2019. **7**(1): p. 102847.
81. Chen, F., et al., Fabrication and characterization of $ZnTiO_3/Zn_2Ti_3O_8$/ZnO ternary photocatalyst for synergetic removal of aqueous organic pollutants and Cr(VI) ions. Sci Total Environ, 2020. **706**: p. 136026.
82. Li, Y., et al., Efficient removal of arsenic from copper smelting wastewater in form of scorodite using copper slag. Journal of Cleaner Production, 2020: p. 122428.
83. Park, B.-Y., et al., Effects of heavy metal contamination from an abandoned mine on nematode community structure as an indicator of soil ecosystem health. Applied Soil Ecology, 2011. **51**: p. 17-24.

84. Yan, B., et al., Leachability characteristic of heavy metals and associated health risk study in typical copper mining-impacted sediments. Chemosphere, 2020. **239**: p. 124748.
85. Hu, H., et al., Synchrotron-based techniques for studying the environmental health effects of heavy metals: Current status and future perspectives. TrAC Trends in Analytical Chemistry, 2020. **122**: p. 115721.
86. Swaidan, A., et al., A facile preparation of CuS-BSA nanocomposite as enzyme mimics: Application for selective and sensitive sensing of Cr(VI) ions. Sensors and Actuators B: Chemical, 2019. **294**: p. 253-262.
87. Wu, H., et al., Heavy Metal(loids) in typical Chinese tobacco-growing soils: Concentrations, influence factors and potential health risks. Chemosphere, 2020. **245**: p. 125591.
88. Wang, L., et al., In vitro oral bioaccessibility investigation and human health risk assessment of heavy metals in wheat grains grown near the mines in North China. Chemosphere, 2020. **252**: p. 126522.
89. Wei, R., et al., Bioaccumulations and potential human health risks assessment of heavy metals in ppk-expressing transgenic rice. Sci Total Environ, 2020. **710**: p. 136496.
90. Demirbas, A., Heavy metal adsorption onto agro-based waste materials: A review. Journal of Hazardous Materials, 2008. **157**(2-3): p. 220-229.
91. Bhatia, P. and M. Nath, Green synthesis of p-NiO/n-ZnO nanocomposites: Excellent adsorbent for removal of congo red and efficient catalyst for reduction of 4-nitrophenol present in wastewater. Journal of Water Process Engineering, 2020. **33**: p. 101017.
92. Bocca, B., et al., Toxic metals contained in cosmetics: a status report. Regul Toxicol Pharmacol, 2014. **68**(3): p. 447-67.
93. Sun, K., et al., Synergistic effect in the reduction of Cr(VI) with Ag-$MoS_2$ as photocatalyst. Applied Materials Today, 2020. **18**: p. 100453.
94. Jia, X., et al., Identification of the potential risk areas for soil heavy metal pollution based on the source-sink theory. J Hazard Mater, 2020. **393**: p. 122424.
95. Ghiloufi, I., L. Khezami, and L. El Mir, Preparation and characterization of nanoporous resin for heavy metal removal from aqueous solution. Journal of Water Supply: Research and Technology-Aqua, 2015. **64**(3): p. 316-325.
96. Ayuso-Alvarez, A., et al., Association between heavy metals and metalloids in topsoil and mental health in the adult population of Spain. Environ Res, 2019. **179**(Pt A): p. 108784.
97. Ugbede, F.O., et al., Natural radionuclides, heavy metals and health risk assessment in surface water of Nkalagu river dam with statistical analysis. Scientific African, 2020: p. e00439.
98. Ma, X.Y., et al., Investigation and assessment of micropollutants and associated biological effects in wastewater treatment processes. Journal of Environmental Sciences, 2020. **94**: p. 119-127.
99. Zhang, X., J. Chen, and J. Li, The removal of microplastics in the wastewater treatment process and their potential impact on anaerobic digestion due to pollutants association. Chemosphere, 2020. **251**: p. 126360.
100. Ahmad, P.T., et al., Efficient reduction of waste water pollution using GO/γ$MnO_2$/Pd nanocomposite as a highly stable and recoverable catalyst. Separation and Purification Technology, 2019. **225**: p. 33-40.
101. Ullah, A., et al., Development of a decision support system for the selection of wastewater treatment technologies. Sci Total Environ, 2020. **731**: p. 139158.

102. Zhang, L., et al., Chemical Characteristics of Precipitation in a Typical Urban Site of the Hinterland in Three Gorges Reservoir, China. Journal of Chemistry, 2018. **2018**: p. 1-10.
103. Pavel, O.D., et al., Catalytic behavior of Li-Al-LDH prepared via mechanochemical and co-precipitation routes for cyanoethylation reaction. Catalysis Today, 2020.
104. Gu, J.-n., et al., Treatment of real deplating wastewater through an environmental friendly precipitation-electrodeposition-oxidation process: Recovery of silver and copper and reuse of wastewater. Separation and Purification Technology, 2020. **248**: p. 117082.
105. Steinbock, O., Complexity from precipitation reactions. Proc Natl Acad Sci U S A, 2014. **111**(49): p. 17346-7.
106. Edañol, Y.D.G., et al., Co-precipitation synthesis of Mg-Al-$CO_3$ layered double hydroxides and its adsorption kinetics with phosphate(V) ions. Materials Today: Proceedings, 2020.
107. Wang, X., et al., Preparation, characterisation, and desalination performance study of cellulose acetate membranes with MIL-53(Fe) additive. Journal of Membrane Science, 2019. **590**: p. 117057.
108. Wang, Z., et al., An electrochemically switched ion exchange process with self-electrical-energy recuperation for desalination. Separation and Purification Technology, 2020. **239**: p. 116521.
109. Olfs, H.W., et al., Comparison of different synthesis routes for Mg–Al layered double hydroxides (LDH): Characterization of the structural phases and anion exchange properties. Applied Clay Science, 2009. **43**(3-4): p. 459-464.
110. Cobzaru, C. and V. Inglezakis, Ion Exchange. 2015: p. 425-498.
111. Kutlu, B., et al., Effects of LDH synthesis and modification on the exfoliation and introduction of a robust anion-exchange procedure. Chemical Engineering Journal, 2014. **243**: p. 394-404.
112. Zewail, T.M. and N.S. Yousef, Kinetic study of heavy metal ions removal by ion exchange in batch conical air spouted bed. Alexandria Engineering Journal, 2015. **54**(1): p. 83-90.
113. Zhao, C., et al., A hybrid process of coprecipitation-induced crystallization-capacitive deionization-ion exchange process for heavy metals removal from hypersaline ternary precursor wastewater. Chemical Engineering Journal, 2019. **378**: p. 122136.
114. Pal, P. and F. Banat, Comparison of heavy metal ions removal from industrial lean amine solvent using ion exchange resins and sand coated with chitosan. Journal of Natural Gas Science and Engineering, 2014. **18**: p. 227-236.
115. Liu, C.-K. and C.-W. Li, Combined electrolysis and micellar enhanced ultrafiltration (MEUF) process for metal removal. Separation and Purification Technology, 2005. **43**(1): p. 25-31.
116. Chen, X., et al., Anti-bacterial performance, disinfection by-products control and optimization strategy in distributed potable water supply using electrolysis. Journal of Cleaner Production, 2020. **265**: p. 121810.
117. Khulbe, K.C. and T. Matsuura, Removal of heavy metals and pollutants by membrane adsorption techniques. Applied Water Science, 2018. **8**(1).
118. Guo, J., et al., ZnS nanoparticles as new additive for polyethersulfone membrane in humic acid filtration. Journal of Industrial and Engineering Chemistry, 2019. **79**: p. 71-78.
119. Kavitha, J., et al., Pretreatment processes for seawater reverse osmosis desalination systems—A review. Journal of Water Process Engineering, 2019. **32**: p. 100926.
120. Landels, A., et al., Improving electrocoagulation floatation for harvesting microalgae. Algal Res, 2019. **39**: p. 101446.

121. Singh, B. and P. Kumar, Pre-treatment of petroleum refinery wastewater by coagulation and flocculation using mixed coagulant: Optimization of process parameters using response surface methodology (RSM). Journal of Water Process Engineering, 2020. **36**: p. 101317.
122. Wei, H., et al., Coagulation/flocculation in dewatering of sludge: A review. Water Res, 2018. **143**: p. 608-631.
123. Nath, A., A. Mishra, and P.P. Pande, A review natural polymeric coagulants in wastewater treatment. Materials Today: Proceedings, 2020.
124. Bruno, P., et al., Bench scale continuous coagulation-flocculation of saline industrial wastewater contaminated by hydrocarbons. Journal of Water Process Engineering, 2020. **34**: p. 101156.
125. Frantz, T.S., et al., Preparation of new biocoagulants by shrimp waste and its application in coagulation-flocculation processes. Journal of Cleaner Production, 2020. **269**: p. 122397.
126. Chen, F., et al., Characteristics and mechanism of chitosan in flocculation for water coagulation in the Yellow River diversion reservoir. Journal of Water Process Engineering, 2020. **34**: p. 101191.
127. Huzir, N.M., et al., Optimization of coagulation-flocculation process for the palm oil mill effluent treatment by using rice husk ash. Industrial Crops and Products, 2019. **139**: p. 111482.
128. Sun, Y., et al., Performance evaluation and optimization of flocculation process for removing heavy metal. Chemical Engineering Journal, 2020. **385**: p. 123911.
129. Choumane, F.Z., et al., Valorisation of a bioflocculant and hydroxyapatites as coagulation-flocculation adjuvants in wastewater treatment of the steppe in the wilaya of Saida (Algeria). Ecological Engineering, 2017. **107**: p. 152-159.
130. Sun, Y., et al., Flocculation activity and evaluation of chitosan-based flocculant CMCTS-g-P(AM-CA) for heavy metal removal. Separation and Purification Technology, 2020. **241**: p. 116737.
131. Kyzas, G. and K. Matis, Flotation in Water and Wastewater Treatment. Processes, 2018. **6**(8): p. 116.
132. Lin, P.-Y., et al., Preparation of vaterite calcium carbonate granules from discarded oyster shells as an adsorbent for heavy metal ions removal. Chemosphere, 2020. **254**: p. 126903.
133. Nageeb, M., Adsorption Technique for the Removal of Organic Pollutants from Water and Wastewater. 2013.
134. Khan, T.A., et al., Removal of Chromium(VI) from aqueous solution using guar gum–nano zinc oxide biocomposite adsorbent. Arabian Journal of Chemistry, 2017. **10**: p. S2388-S2398.
135. Wen, X.J., et al., Photocatalytic degradation of sulfamethazine using a direct Z-Scheme AgI/$Bi_4V_2O_{11}$ photocatalyst: Mineralization activity, degradation pathways and promoted charge separation mechanism. J Hazard Mater, 2020. **385**: p. 121508.
136. Ma, X., et al., A novel nitrogen-deficient g-$C_3N_4$ photocatalyst fabricated via liquid phase reduction route and its high photocatalytic performance for hydrogen production and Cr(VI) reduction. Materials Research Bulletin, 2020. **129**: p. 110909.
137. Xiao, Y., et al., Synthesis of EDTA-bridged CdS/g-$C_3N_4$ heterostructure photocatalyst with enhanced performance for photoredox reactions. J Colloid Interface Sci, 2020. **577**: p. 459-470.

138. He, H.Y., Efficient interface-induced effect of novel reduced graphene oxide-CoS heteronanostructures in enhancing photocatalytic acitivities. Applied Surface Science, 2017. **421**: p. 260-267.
139. Hosseinpour, Z., Z. Arefinia, and S. Hosseinpour, Cu doped cubic pyrite-type $CoS_2$ ball like superstructures as heterogeneous photocatalyst. Materials Chemistry and Physics, 2018. **220**: p. 426-432.
140. Xin, Y., Q. Chen, and G. Zhang, Construction of ternary heterojunction CuS-CdS/$TiO_2$ nanobelts for photocatalytic degradation of gaseous toluene. Journal of Alloys and Compounds, 2018. **751**: p. 231-240.
141. Xu, T., et al., Solar-driven conversion of arylboronic acids to phenols using metal-free heterogeneous photocatalysts. Journal of Catalysis, 2019. **378**: p. 63-67.
142. Wetchakun, K., N. Wetchakun, and S. Sakulsermsuk, An overview of solar/visible light-driven heterogeneous photocatalysis for water purification: $TiO_2$- and ZnO-based photocatalysts used in suspension photoreactors. Journal of Industrial and Engineering Chemistry, 2019. **71**: p. 19-49.
143. Yu, Z., et al., Synthesis of high efficient and stable plasmonic photocatalyst Ag/$AgNbO_3$ with specific exposed crystal-facets and intimate heterogeneous interface via combustion route. Applied Surface Science, 2019. **488**: p. 485-493.
144. Tahir, M.B., et al., Fabrication of heterogeneous photocatalysts for insight role of carbon nanofibre in hierarchical $WO_3$/ $MoSe_2$ composite for enhanced photocatalytic hydrogen generation. Ceramics International, 2019. **45**(5): p. 5547-5552.
145. Shahzad, K., et al., Role of $CuCo_2S_4$ in Z-scheme $MoSe_2$/$BiVO_4$ composite for efficient photocatalytic reduction of heavy metals. Ceramics International, 2019. **45**(17): p. 23225-23232.
146. Li, M., et al., Novel Z-scheme visible-light photocatalyst based on $CoFe_2O_4$/BiOBr/Graphene composites for organic dye degradation and Cr(VI) reduction. Applied Surface Science, 2019. **478**: p. 744-753.
147. Li, S., et al., Adsorption and mechanistic study of the invasive plant-derived biochar functionalized with CaAl-LDH for Eu(III) in water. Journal of Environmental Sciences, 2020. **96**: p. 127-137.
148. Wijitwongwan, R., S. Intasa-ard, and M. Ogawa, Preparation of Layered Double Hydroxides toward Precisely Designed Hierarchical Organization. ChemEngineering, 2019. **3**(3): p. 68.
149. Zhou, H., Z. Jiang, and S. Wei, A new hydrotalcite-like absorbent FeMnMg-LDH and its adsorption capacity for $Pb^{2+}$ ions in water. Applied Clay Science, 2018. **153**: p. 29-37.
150. Jafari Foruzin, L., et al., High quantum efficiency of photocatalytic water oxidation over the $TiO_2$/MMO nanocomposite under visible-light irradiation. Journal of Molecular Liquids, 2019. **288**: p. 111035.
151. Qiu, C., et al., 2-Methylimidazole directed ambient synthesis of zinc-cobalt LDH nanosheets for efficient oxygen evolution reaction. J Colloid Interface Sci, 2020. **565**: p. 351-359.
152. Zhang, S., et al., Oxygen vacancies engineering in $TiO_2$ homojunction/ZnFe-LDH for enhanced photoelectrochemical water oxidation. Chemical Engineering Journal, 2020. **395**: p. 125101.
153. Ghanbari, M., F. Soofivand, and M. Salavati-Niasari, Simple synthesis and characterization of $Ag_2$ $CdI_4$ /AgI nanocomposite as an effective photocatalyst by co-precipitation method. Journal of Molecular Liquids, 2016. **223**: p. 21-28.

154. Wang, W., et al., Cr(VI) removal from aqueous solutions by hydrothermal synthetic layered double hydroxides: Adsorption performance, coexisting anions and regeneration studies. Colloids and Surfaces A: Physicochemical and Engineering Aspects, 2014. **457**: p. 33-40.
155. Ma, X., et al., Hydrothermal preparation and anion exchange of $Co^{2+}$–$Ni^{2+}$–$Fe^{3+}$ $CO_3^{2-}$ LDHs materials with well regular shape. Colloids and Surfaces A: Physicochemical and Engineering Aspects, 2010. **371**(1-3): p. 71-75.
156. Tzompantzi, F., et al., Enhanced photoactivity for the phenol mineralization on ZnAlLa mixed oxides prepared from calcined LDHs. Catalysis Today, 2014. **220-222**: p. 56-60.
157. Ni, J., et al., Fabrication of ZnAl mixed metal-oxides/RGO nanohybrid composites with enhanced photocatalytic activity under visible light. Applied Surface Science, 2018. **441**: p. 599-606.
158. Chivu, V., et al., Heterostructures of Ce-Ti/layered double hydroxides and the derived MMOs for photoenergy applications. Applied Surface Science, 2020. **513**: p. 145853.
159. Kim, S., et al., Enhanced photocatalytic ability of Cu, Co doped ZnAl based mixed metal oxides derived from layered double hydroxides. Colloids and Surfaces A: Physicochemical and Engineering Aspects, 2017. **524**: p. 43-52.
160. Xue, B., et al., AgI/$TiO_2$ nanocomposites: ultrasound-assisted preparation, visible-light induced photocatalytic degradation of methyl orange and antibacterial activity. Ultrason Sonochem, 2015. **22**: p. 1-6.
161. Thanh Tung, M.H., et al., Novel direct Z-scheme AgI/N–$TiO_2$ photocatalyst for removal of polluted tetracycline under visible irradiation. Ceramics International, 2020. **46**(5): p. 6012-6021.
162. Qin, J., et al., A novel Z-scheme $Ag_6Si_2O_7$/AgI nanocomposite photocatalyst: Study on the degradation of various refractory compounds and reduction of vanadium (V). Journal of Alloys and Compounds, 2020. **815**: p. 152706.
163. Wang, L., et al., Controlling wettability of AgI/$BiVO_4$ composite photocatalyst and its effect on photocatalytic performance. Journal of Alloys and Compounds, 2020. **835**: p. 155367.
164. Lakhera, S.K., et al., Fabrication of high surface area AgI incorporated porous $BiVO_4$ heterojunction photocatalysts. Materials Science in Semiconductor Processing, 2020. **106**: p. 104756.
165. Shaker-Agjekandy, S. and A. Habibi-Yangjeh, Facile one-pot method for preparation of AgI/ZnO nanocomposites as visible-light-driven photocatalysts with enhanced activities. Materials Science in Semiconductor Processing, 2015. **34**: p. 74-81.
166. Olivera, S., et al., Potential applications of cellulose and chitosan nanoparticles/composites in wastewater treatment: A review. Carbohydr Polym, 2016. **153**: p. 600-618.
167. Renu, M. Agarwal, and K. Singh, Heavy metal removal from wastewater using various adsorbents: a review. Journal of Water Reuse and Desalination, 2017. **7**(4): p. 387-419.
168. Shankar, S., A.A. Oun, and J.W. Rhim, Preparation of antimicrobial hybrid nano-materials using regenerated cellulose and metallic nanoparticles. Int J Biol Macromol, 2018. **107**(Pt A): p. 17-27.
169. Li, H., et al., Hierarchically porous $MoS_2$ /CoAl-LDH/HCF with synergistic adsorption-photocatalytic performance under visible light irradiation. Journal of Alloys and Compounds, 2017. **698**: p. 852-862.

170. Huo, R., et al., Enhanced photocatalytic performances of hierarchical $ZnO/ZnAl_2O_4$ microsphere derived from layered double hydroxide precursor spray-dried microsphere. J Colloid Interface Sci, 2013. **407**: p. 17-21.
171. Elhalil, A., et al., Photocatalytic degradation of caffeine by $ZnO\text{-}ZnAl_2O_4$ nanoparticles derived from LDH structure. Journal of Environmental Chemical Engineering, 2017. **5**(4): p. 3719-3726.

## 7. Appendix

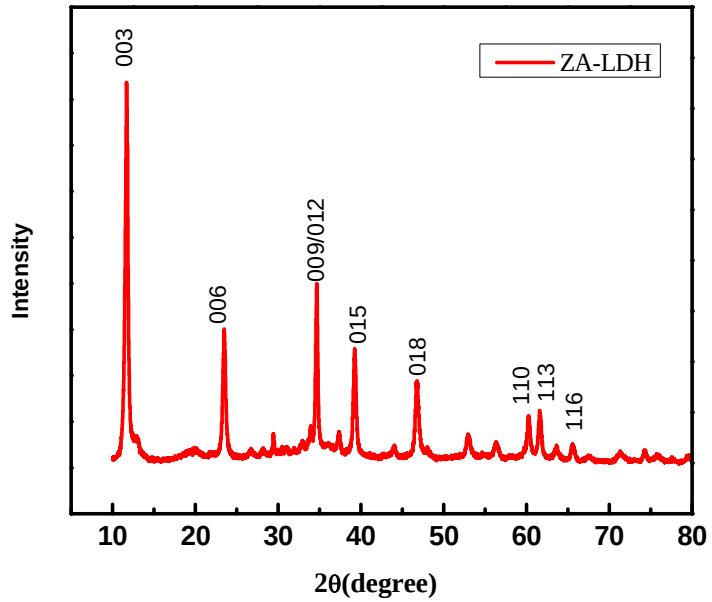


Appendix 1. Zn/Al LDH RD analysis

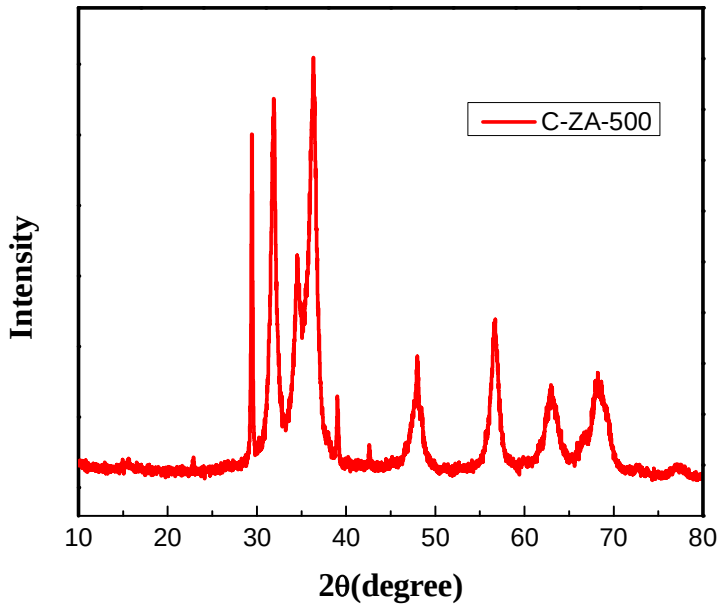


Appendix 2. Cellulose templated Zn/Al LDH XRD peak analysis calcined at 500℃

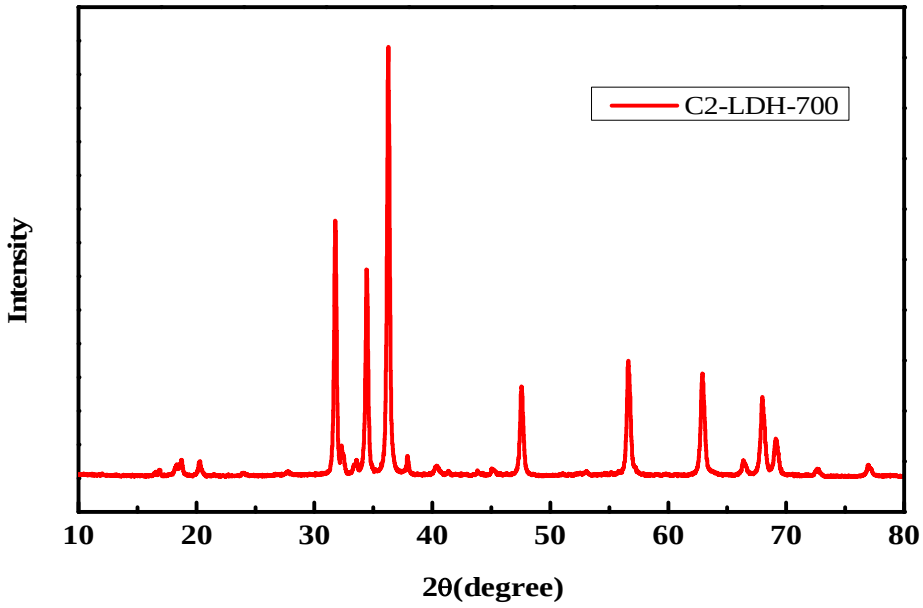


Appendix 3. Zn/Al LDH XRD peak analysis calcined at 700℃

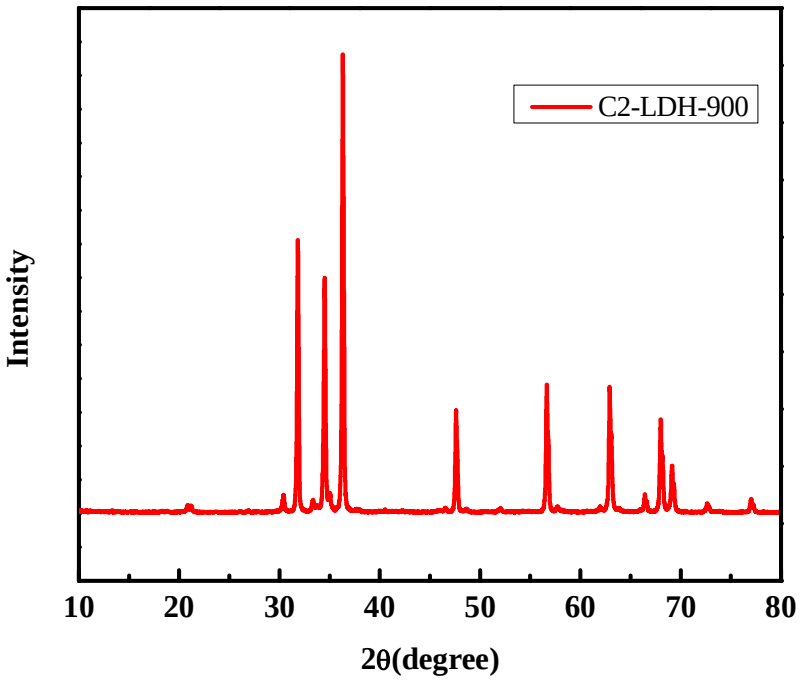


Appendix 4. Cellulose templated Zn/Al LDH XRD peak analysis calcined at 900℃

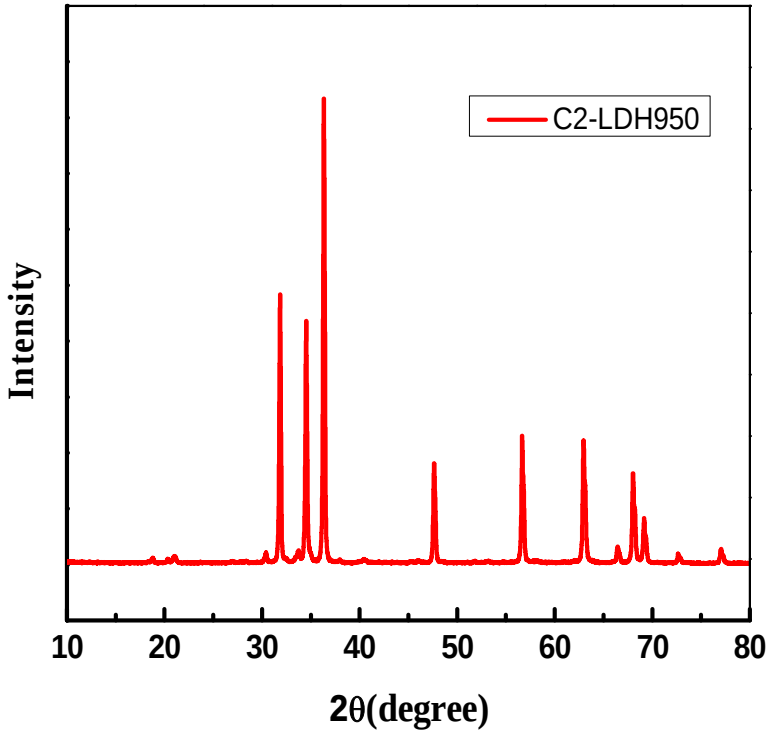


Appendix 5. Cellulose templated Zn/Al LDH XRD peak analysis calcined at 950℃

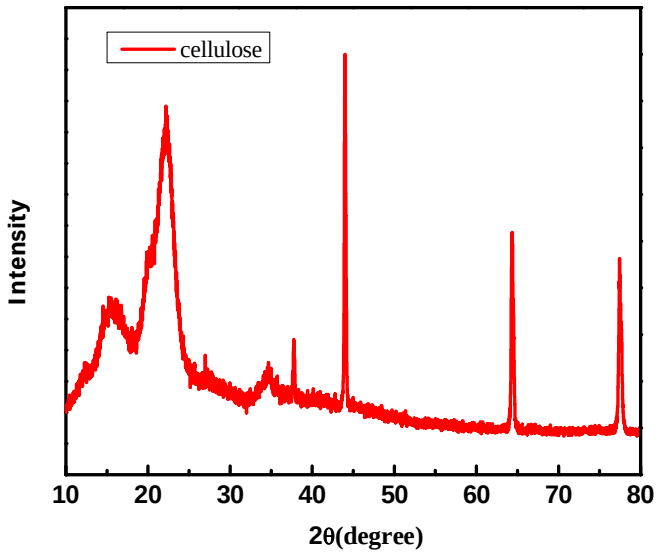


Appendix 6 SCB crystalline Micro-cellulose XRD analysis

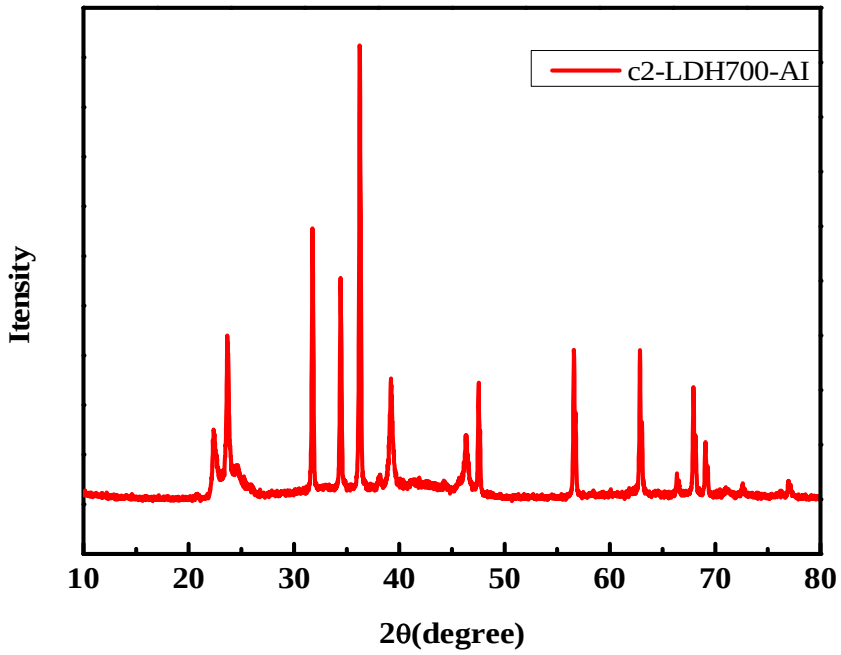


Appendix 7. Cellulose templated Zn/Al LDH/AgI composite XRD analysis calcined at 700℃

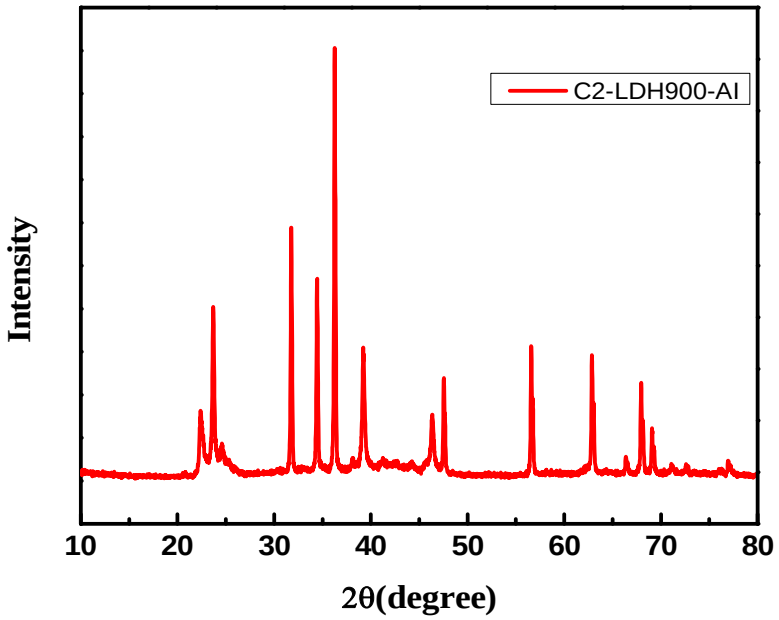


Appendix Figure 8. Cellulose templated Zn/Al LDH/AgI XRD analysis calcined at 900℃

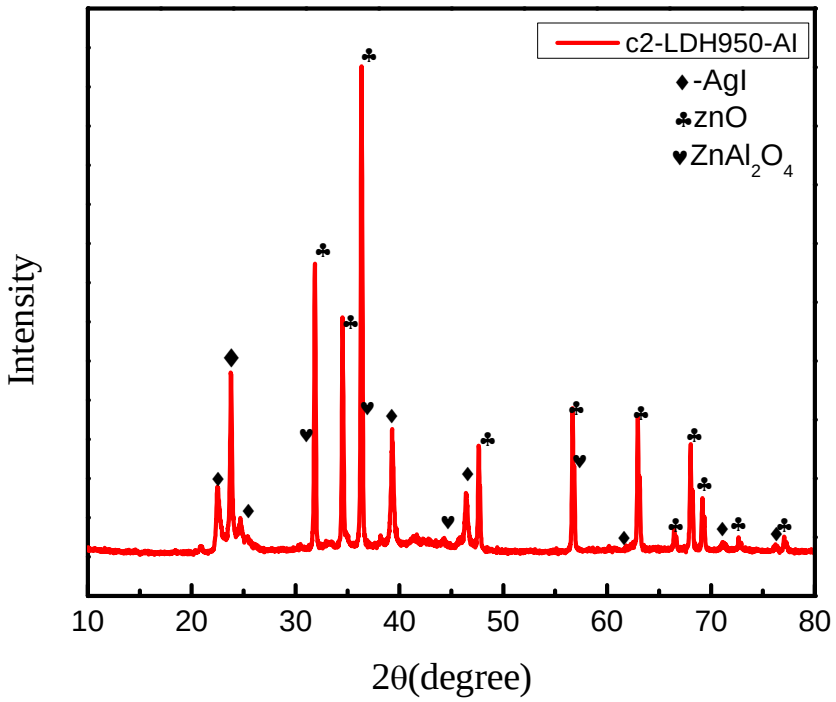


Appendix 8. Cellulose templated Zn/Al LDH/AgI composite XRD analysis calcined at 950℃

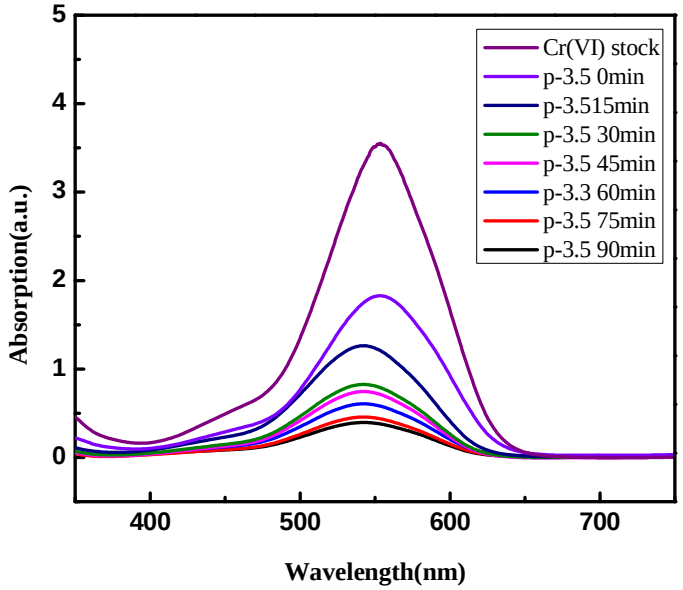


Appendix 9. pH factor on the photocatalyst reduction of Cr(VI) at PH=3.5